ION/MOLECULE REACTIONS STUDIED WITH THE FLOWING AFTERGLOW AND THEORETICAL METHODOLOGY

by

Kyle Richard Tilger

B. A., Washington and Jefferson College, 2002

Submitted to the Graduate Faculty of

Arts and Sciences in partial fulfillment

of the requirements for the degree of

Master of Science

University of Pittsburgh

2006

UNIVERSITY OF PITTSBURGH

FACULTY OF ARTS AND SCIENCES

This thesis was presented

by

Kyle Richard Tilger

It was defended on

April 21, 2006

and approved by

Kenneth D. Jordan

Peter E. Siska

Thesis Advisor: Dr. Joseph J. Grabowski

ION/MOLECULE REACTIONS STUDIED WITH THE FLOWING AFTERGLOW AND THEORETICAL METHODOLOGY

Kyle Richard Tilger, M.S.

University of Pittsburgh, 2006

Initial interest in ion/molecule chemistry was because of its importance in atmospheric chemistry, but researchers have moved to investigating other interests involving organic reaction mechanisms. The study of ion/molecule reactions has flourished with the invention of instruments, such as the flowing afterglow instrument, and the advances in computational chemistry.

The hydronium ion has been utilized as a reagent ion in ion/molecule chemistry for the detection of volatile organic compounds (VOCs). A limitation to the utility of the hydronium ion is that it is susceptible to clustering reactions with water. The propensity to cluster can be eliminated by replacing the hydrogens on the hydronium ion with trimethylsilyl groups to form the tris-trimethylsilyloxonium ion, $(TMS)_3O^+$. This strategy takes advantage of the trimethylsilyl cation's proclivity to react as if it were a proton.

Hexamethyldisiloxane was allowed to react with TMS^+, $(TMS)_2Cl^+$, $TMSOH_2^+$, and $TMSC_6H_6^+$ in an attempt to form $(TMS)_3O^+$. However, every attempt to create the novel $(TMS)_3O^+$ via a gas phase approach was unsuccessful. The available data suggests that the target ion may be formed, but is so reactive under the experimental conditions that it reacts away prior to detection.

An investigation of the formation and reactions of the bis-trimethylsilylmethyloxonium ion ($(TMS)_2OCH_3^+$) was conducted to gain further understanding of the chemistry of the formation and reactivity of oxonium ions. After successful formation of the bis-trimethylsilylmethyloxonium ion, six neutrals (water, dimethylsulfide, acetonitrile, ethyl acetate, triethylamine, and acetone) were allowed to react one at a time with it. Trimethylsilyl transfer was the primary reaction pathway, which bodes well for our goal of creating a novel reagent ion.

The oxygen radical anion, $O^{\cdot-}$, has been studied by others with respect to atmospheric chemistry and has been utilized for chemical ionization reactions. To better understand its reactivity, a theoretical study of the reaction of the $O^{\cdot-}$ with methanol has been analyzed. Reaction schemes and potential energy diagrams for observable products and for all possible products were created. The potential energy surface computed during this study suggests that at 298 K the expected product distribution is proton transfer.

TABLE OF CONTENTS

LIST OF TABLES

LIST OF FIGURES

LIST OF SCHEMES

PREFACE

First, I would like to thank Dr. Joseph Grabowski, my advisor, for all of his time, support, and encouragement. I would like to recognize my committee members, Dr. Kenneth Jordan and Dr. Peter Siska, for their time and suggestions. Thank you to Gab-Yong Lee for allowing me to use his data from the theoretical study of the reaction of the oxygen radical anion with methanol. I would like to thank Mark Morris for all of his advice along the path to my degree. I would also like to acknowledge my group members, Christopher Taormina, Mingxiang Lin, Kevin Davies, and Thomas Watson for their support. Thank you to my parents Kenneth and Marjorie, my brother Ken, my grandmother Margaret, and the rest of my family who have always supported and encouraged me in all of my educational pursuits. Special thanks goes to my fiancé and soon to be wife, Alissa Lipchick, who would always listen to me when I was discouraged and offer emotional support. Finally, I would like to thank Alissa's family (John, Angela, John, Joe, etc…) and all of my friends, especially Amanda Garner, Brian Johnson, Francis Burt, and Craig Chess, who have always been there for me while I attended graduate school.

1.0 INTRODUCTION

1.1 ION/MOLECULE CHEMISTRY

In 1925 the first ion/molecule reaction was performed; however, not much work was performed in this field until approximately 30 years later.[1,2] One reason that ion/molecule chemistry became a focus of researchers is because of its importance in atmospheric chemistry.[3] Technological advances, such as the creation of the flowing afterglow, provided researchers with the tools necessary to explore ion-molecule reactions.[4] Many of the chemical processes occurring in our atmosphere are well understood and explained because of ion/molecule reactions performed with this technology.[5]

1.2 FLOWING AFTERGLOW

In the 1960's the flowing afterglow method was developed by Ferguson, Fehsenfeld, Schmeltekopf, and coworkers at the National Oceanic and Atmospheric Administration Laboratories.[4] Originally this technique was developed for the study of reactions occurring in the earth's atmosphere, but since then the technique has been utilized for other types of studies. Some examples are organic reaction mechanisms and ion solvation phenomenon.[6,7]

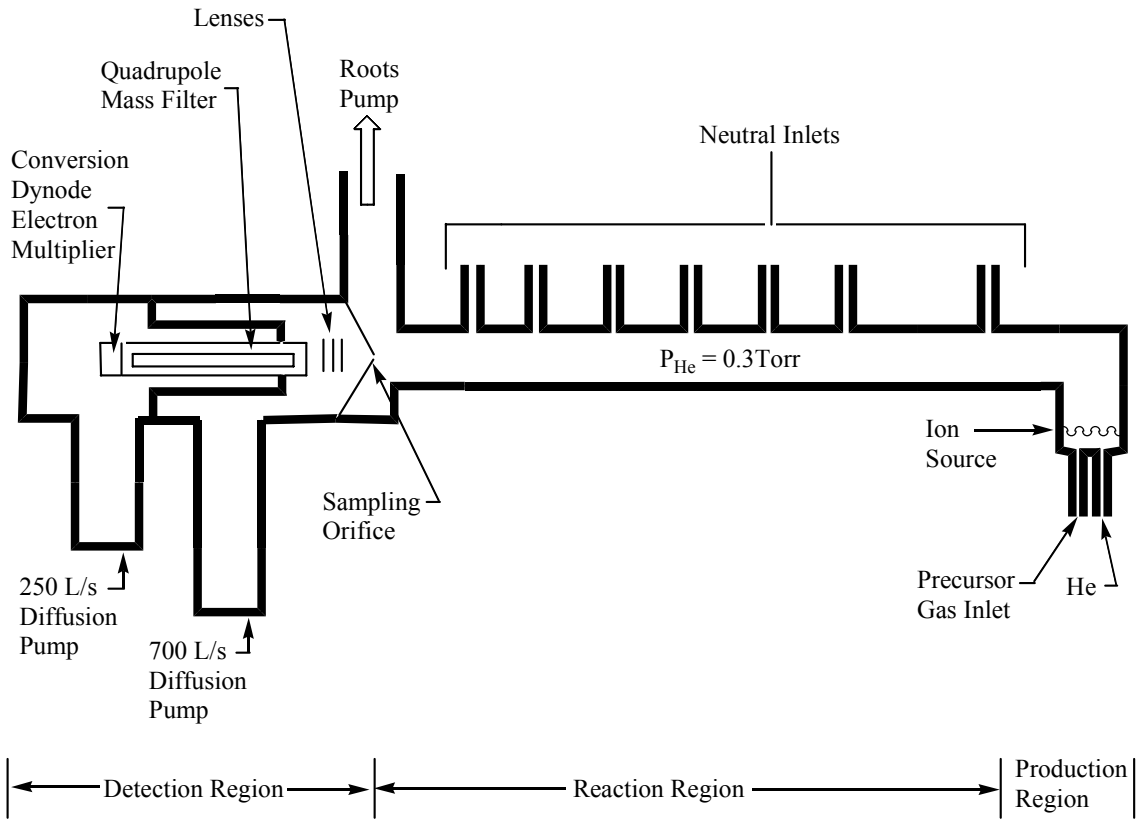

Figure 1.1 Schematic of the Flowing Afterglow

Figure 1.1 depicts a flowing afterglow apparatus. In the production region, both helium gas and a precursor gas are introduced. The precursor gas is ionized in the ion source and the He is used as a buffer gas to thermalize and carry the ions from the production region. Next, the ions flow thru the reaction region where neutral reagents are introduced and allowed to react with these ions which were created upstream. At the end of the reaction region, a portion of the ions remaining from the reactions in the flow tube are directed through the sampling orifice by an electrical field while the roots pump removes most of the helium. After passing through the sampling orifice, the ions are directed by lenses into a quadrupole mass filter. Finally after passing through the quadrupole mass filter, the ions reach a detector.

1.3 COMPUTATIONAL CHEMISTRY

The advancement of computational chemistry has been beneficial to gas-phase ion-molecule chemistry. The ability to model complex molecules and gas phase reactions accurately and efficiently has increased with the creation of powerful programs like Gaussian and CAChe along with the increased processing power of computers.[8,9] Because many of the experiments performed in ion/molecule chemistry are under low pressure, the experimental conditions are close to a truly isolated system, which can be the conditions used by the theory programs.[10] This makes molecular orbital and density functional theory calculations ideal for modeling gas-phase ion chemistry.

Computational work has been used to predict thermodynamic stability of species never synthesized, guide experimental work, and clarify structure and properties of non-conventional species.[11] An example of a molecule that were predicted to exist theoretically before being discovered experimentally is ammonia oxide.[11] Theoretical methods have also been used in tandem with other techniques to aid in the explanation of experimental products observed.[12]

2.0 THE TRIS-TRIMETHYLSILYLOXONIUM ION

2.1 INTRODUCTION

The hydronium ion has been utilized as a reagent ion for the detection of volatile organic compounds (VOCs).[13] One limitation of using this ion is that it is susceptible to clustering reactions, which can complicate analysis of results. One way to eliminate this clustering limitation is to replace the hydrogen in the hydronium ion with trimethylsilyl groups (Figure 2.1) to form the tris-trimethylsilyloxonium ion (*m/z* 235). Trimethylsilyl groups have been chosen

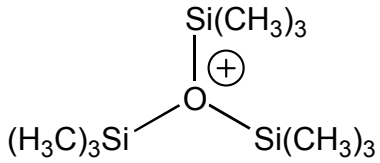

Figure 2.1 Tris-trimethylsilyloxonium Ion

because the trimethylsilyl cation is similar in reactivity to a proton and has even been referred to as a "large proton".[14] This idea was tested by Hwu and Wetzel who showed that Me_3SiOTf can be used as an acid to catalyze a dioxolanation reaction.[15] By using Me_3SiOTf and 1,2-bis[(trimethylsilyl)oxy]ethane, they were able to differentiate between two carbonyl groups by

taking advantage of steric effects. By doing so it was possible to selectively put a protecting group on a desired carbonyl.

The formation of the tris-trimethylsilyloxonium ion has been reported in the condensed phase by Olah et al.[16] Trityl-TPFPB salt, $Ph_3C^+B(C_6F_5)_4^-$, was allowed to react with trimethylsilane in the presence of hexamethyldisiloxane at -78°C to form the tris-trimethylsilyloxonium ion. The ion's structure was confirmed by ^{29}Si, ^{1}H, and ^{13}C NMR spectroscopy at -70°C.[16] The HF/6-31G* optimized geometry shown in Figure 2.2 is in agreement with their experimental data.[16] To the best of my knowledge, this ion has not been reported as having been studied or formed in the gas phase.

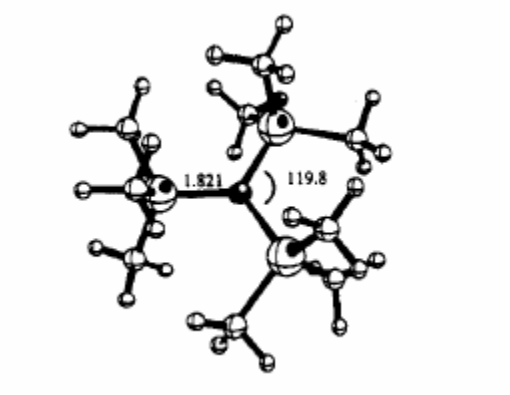

Figure 2.2 HF/6-31G* Optimized Geometry of $(TMS)_3O^+$ [16]

2.2 EXPERIMENTAL

The flowing afterglow system has been described in detail; only unique aspects relevant to this work will be reported here.[17] Helium pressures were maintained near 0.3 Torr for each of the reactions examined. The reagents used without further purification were oxygen (grade 2.6,

Valley National Gas, Pittsburgh, PA), tetramethylsilane (99.9%, Sigma Aldrich), trimethylsilyl chloride (99.0%, Sigma Aldrich), benzene (99.9% HPLC Grade, Fisher Scientific), and hexamethyldisiloxane (98% Sigma Aldrich). Qualitative experiments were performed to determine the *m/z* of the ionic products of the studied reactions. Since the desired ion was never detected, the reaction rate constants and branching ratios were not pursued.

2.3 RESULTS

In the first attempt to form the tris-trimethylsilyloxonium ion (Equations 2.1-2.3), oxygen was ionized at the ion source to form $O_2^{\cdot+}$, which was then allowed to react with tetramethylsilane to form the trimethylsilyl cation. The trimethylsilyl cation was allowed to react with hexamethyldisiloxane in an attempt to form the tris-trimethylsilyloxonium ion. The reaction distance was varied from 76.7 to 16.1 cm at 10.1 cm distances, and the pressure of hexamethyldisiloxane was varied from 0 to 2 Torr in an effort to form the ion being sought. The only product ion detected was *m/z* 163, which had an isotopic distribution that corresponded to protonated hexamethyldisiloxane as shown in Table 2.1.

Table 2.1 Isotopic Distribution for the Reaction of Me_3Si^+ with Hexamethyldisiloxane

m/z	Theoretical	Observed
163	100.0	100.0
164	16.8	16.3
165	8.0	7.8
166	0.8	0.9
167	0.1	0.1

$$O_2 \xrightarrow[0.3\ \text{Torr He}]{\text{ei/pi}} O_2^{\cdot +} \qquad \textbf{2.1}$$

$$O_2^{\cdot +} \xrightarrow{Me_4Si} Me_3Si^+ + Me^{\cdot} + O_2 \qquad \textbf{2.2}$$

$$Me_3Si^+ \xrightarrow{(Me_3Si)_2O} \left[(Me_3Si)_3O^+\right] \xrightarrow{(Me_3Si)_2O} (Me_3Si)_2OH^+ + (Me_3Si)_2O + Me_2SiCH_2 \qquad \textbf{2.3}$$

In a second approach to forming the tris-trimethylsilyloxonium ion, the bis-trimethylsilyl chloronium ion was formed by electron ionization and penning ionization of trimethylsilyl chloride at the ion source and allowing it to react with trimethylsilyl chloride in the flow tube. Next the bis-trimethylsilyl chloronium ion was allowed to react with hexamethyldisiloxane (Equations 2.4-2.6). Up to 1.5 Torr of hexamethyldisiloxane was added and the reaction distance was varied from 76.7 to 16.1 cm in an effort to form the tris-trimethyloxonium ion. The product ion was *m/z* 163, and is hypothesized to be protonated hexamethyldisiloxane.

$$Me_3SiCl \xrightarrow[0.3\ \text{Torr He}]{\text{ei/pi}} Me_3Si^+ + Cl^- \qquad \textbf{2.4}$$

$$Me_3Si^+ \xrightarrow{Me_3SiCl} (Me_3Si)_2Cl^+ \qquad \textbf{2.5}$$

$$(Me_3Si)_2Cl^+ \xrightarrow{(Me_3Si)_2O} (TMS)_2OH^+ + (CH_3)_3SiCl + (CH_3)_2SiCH_2 \qquad \textbf{2.6}$$

In a third attempt to form the tris-trimethylsilyloxonium ion, the protonated form of trimethylsilanol was created by allowing $O_2^{\cdot +}$ to react with tetramethylsilane to form the

trimethylsilyl cation, and then allowing that ion to react with water (equations 2.1, 2.2, 2.7).[18] Protonated trimethylsilanol was also allowed to react with hexamethyldisiloxane in an attempt to form the tris-trimethylsilyloxonium ion (equation 2.8). This also gave a product ion at *m/z* 163, which according to the isotopic distributions in Table 2.2 corresponds to protonated hexamethyldisiloxane.

Table 2.2 Isotopic Distribution for the Reaction of $Me_3SiOH_2^+$ with Hexamethyldisiloxane

m/z	Theoretical	Observed
163	100.0	100.0
164	16.8	16.0
165	8.0	8.4
166	0.8	0.9
167	0.1	0.1

$$Me_3Si^+ \xrightarrow[He]{H_2O} Me_3SiOH_2^+ \qquad \textbf{2.7}$$

$$Me_3SiOH_2^+ \xrightarrow{(Me_3Si)_2O} (Me_3Si)_2OH^+ + Me_3SiOH \qquad \textbf{2.8}$$

Table 2.3 Isotopic Distribution for the Reaction of $Me_3SiC_6H_6^+$ with Hexamethyldisiloxane

m/z	Theoretical	Observed
163	100.0	100.0
164	16.8	16.1
165	8.0	8.8
166	0.8	0.9
167	0.1	0.1

$$Me_3Si^+ \xrightarrow{C_6H_6} Me_3SiC_6H_6^+ \qquad \textbf{2.9}$$

$$Me_3SiC_6H_6^+ \xrightarrow{(Me_3Si)_2O} (Me_3Si)_2OH^+ + Me_3SiC_6H_5 \qquad \textbf{2.10}$$

Finally, the trimethylsilyl cation, formed from the reaction of $O_2^{\cdot+}$ and tetramethylsilane, was allowed to react with benzene to form the trimethylsilyl adduct (equations 2.1, 2.2, 2.9). This latter ion was then allowed to react with hexamethyldisiloxane (equation 2.10). The product ion observed at *m/z* 163 was protonated hexamethyldisiloxane.

2.4 DISCUSSION

The reaction of the trimethylsilyl cation and hexamethyldisiloxane was designed to mimic the reaction of the trimethylsilyl cation with water. In that reaction, $TMSOH_2^+$ is formed at a rate close to the collisional rate of 2 x 10^{-9} cm^3 $molecule^{-1}$ s^{-1}.[18] However, the reaction of the trimethylsilyl cation with hexamethyldisiloxane did not produce the cluster ion, instead protonated hexamethyldisiloxane was formed. While it remains uncertain as to how *m/z* 163 is formed, it is possible that it is formed as a secondary product from the reaction of the target ion ($(TMS)_3O^+$) with hexamethyldisiloxane as summarized in equations 2.1-2.3.

Squires et al. formed the trimethyloxonium ion in the gas phase at 298 K using a flowing afterglow apparatus by allowing $Cl(CH_3)_2^+$ to react with $(CH_3)_2O$.[19] However in our hands an analogous approach by allowing $Cl(Si(CH_3)_3)_2^+$ to react with $O(Si(CH_3)_3)_2$ did not result in the formation of the tris-trimethylsilyloxonium ion. Instead of the desired ion, protonated

hexamethyldisiloxane was observed which indicates the E2 reaction summarized in equation 2.6 is occurring instead of the trimethylsilyl transfer reaction.

In the reaction of the trimethylsilyl cation with hexamethyldisiloxane, proton transfer is endothermic by 24 kcal/mol.[20] Since endothermic reactions are too slow to be observed in the time window accessible to ion/molecule reactions studied in the flowing afterglow, a different pathway must be occurring. While we did not pursue the other pathway because our interest was in the tris-trimethylsilyloxonium ion, it is possible that the target was made but is so reactive that it does an E2 under our reaction conditions before we can detect it. This possibility will be explored in the future.

2.5 CONCLUSIONS

A successful way of creating the tris-trimethylsilyloxonium ion in the gas phase has yet to be discovered. In solution the tris-trimethylsilyloxonium ion has a stabilizing counterpart; however, to form it in the gas phase there is not a stabilizing counter ion. The lack of that stabilizing ion may make the formation of the tris-trimethylsilyloxonium ion thermo chemically unstable. Another reason for the lack of observing of the tris-trimethylsilyloxonium ion may be the existence of another reaction pathway that is kinetically faster. More studies are necessary to elucidate the chemistry of the formation process of this ion.

3.0 THE BIS-TRIMETHYLSILYLMETHYLOXONIUM ION

3.1 INTRODUCTION

An investigation of the formation and reactions of the bis-trimethylsilylmethyloxonium ion (*m/z* 177), shown in Figure 3.1 below, was conducted. $(TMS)_2OCH_3^+$ was chosen for study as a possible reagent ion for VOC detection. Studying the reactions of $(TMS)_2OCH_3^+$ will provide information as to how different substituents affect the reactivity and selectivity of onium ions. It was hypothesized that the ion would have two dominant reaction pathways, methyl transfer and trimethylsilyl transfer.

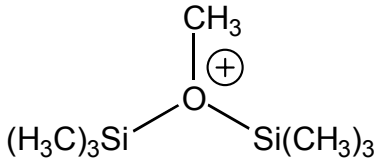

Figure 3.1 Bis-trimethylsilylmethyloxonium Ion

3.2 EXPERIMENTAL

Qualitative experiments were performed to determine the *m/z* of the products of ion/molecule reactions. Rate coefficients were determined by examining the change in reactant ion as the concentration of neutral was altered. Measurements of the rate coefficients were performed at least five times over two experimental days, with an experimental day being defined as the complete startup and shutdown of the instrument. Helium pressures were maintained near 0.3 Torr for each of the reactions examined. The reagents used are: argon (grade 4.8, Valley National Gas, Pittsburgh, PA), tetramethylsilane (99.9%, Sigma Aldrich), methoxytrimethylsilane (99%, Sigma Aldrich), deionized water, acetone (99%, Fisher Scientific, Pittsburgh, PA), triethylamine (99%, Fisher Scientific, Pittsburgh, PA), dimethylsulfide (99+%, Sigma Aldrich), acetonitrile (99%, Fisher Scientific, Pittsburgh, PA), and ethyl acetate (99.9% HPLC Grade, Fisher Scientific). All of the liquid reagents were freeze-pump-thawed to remove dissolved gases prior to use.

3.3 RESULTS

Ar^+, formed by ionizing argon at the source, was allowed to react with tetramethylsilane to form the trimethylsilyl cation, which was then allowed to react with methoxytrimethylsilane giving the desired bis-trimethylsilylmethyloxonium ion (equation 3.1 – 3.3). The reaction of the trimethylsilyl cation and methoxytrimethylsilane went to completion, and the pressure independent rate constant was measured at 8.00×10^{-10} cm^3 $molecule^{-1}$ s^{-1} with 4.6% standard deviation. The experimental isotopic distribution shown in Figure 3.2 matches the theoretical

$$Ar \xrightarrow[0.3\ Torr\ He]{ei/pi} Ar^+ \qquad \textbf{3.1}$$

$$Ar^+ \xrightarrow{(CH_3)_4Si} (CH_3)_3Si^+ + CH_3 + Ar \qquad \textbf{3.2}$$

$$(CH_3)_3Si^+ \xrightarrow[He]{(CH_3)_3SiOCH_3} ((CH_3)_3Si)_2OCH_3^+ \qquad \textbf{3.3}$$

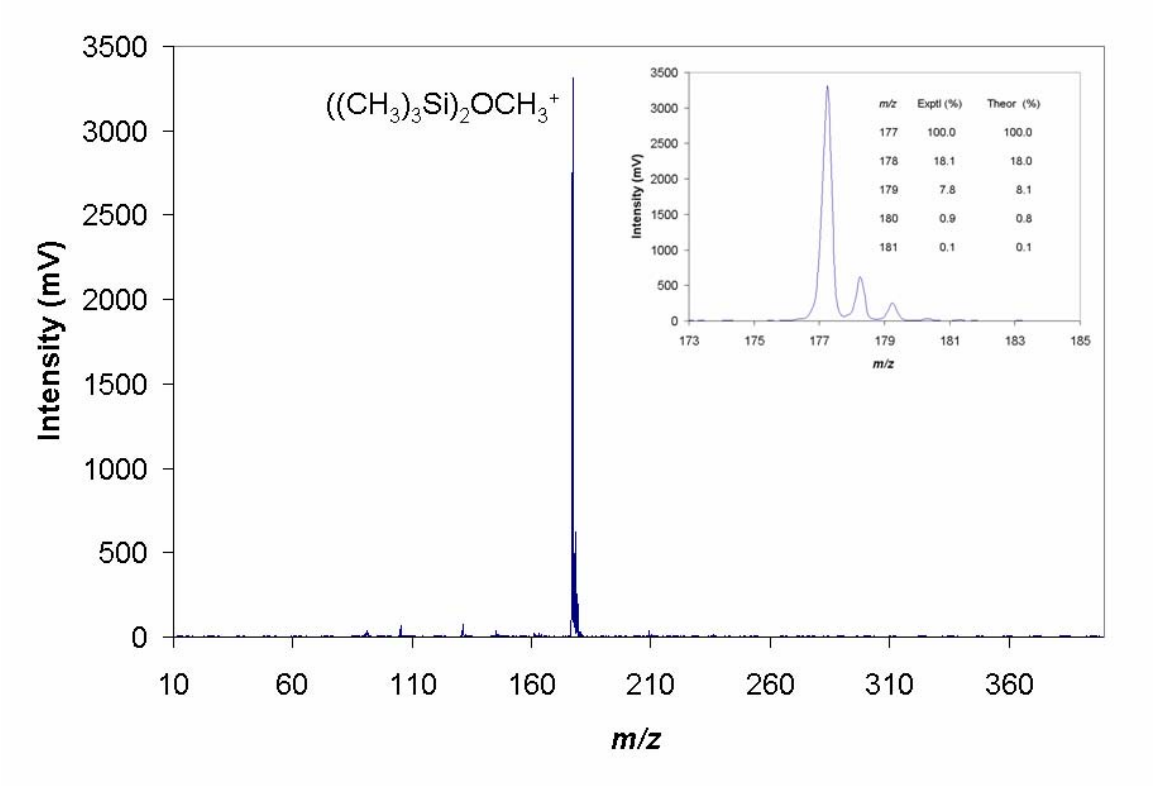

Figure 3.2 Bis-trimethylsilylmethyloxonium Ion Spectrum

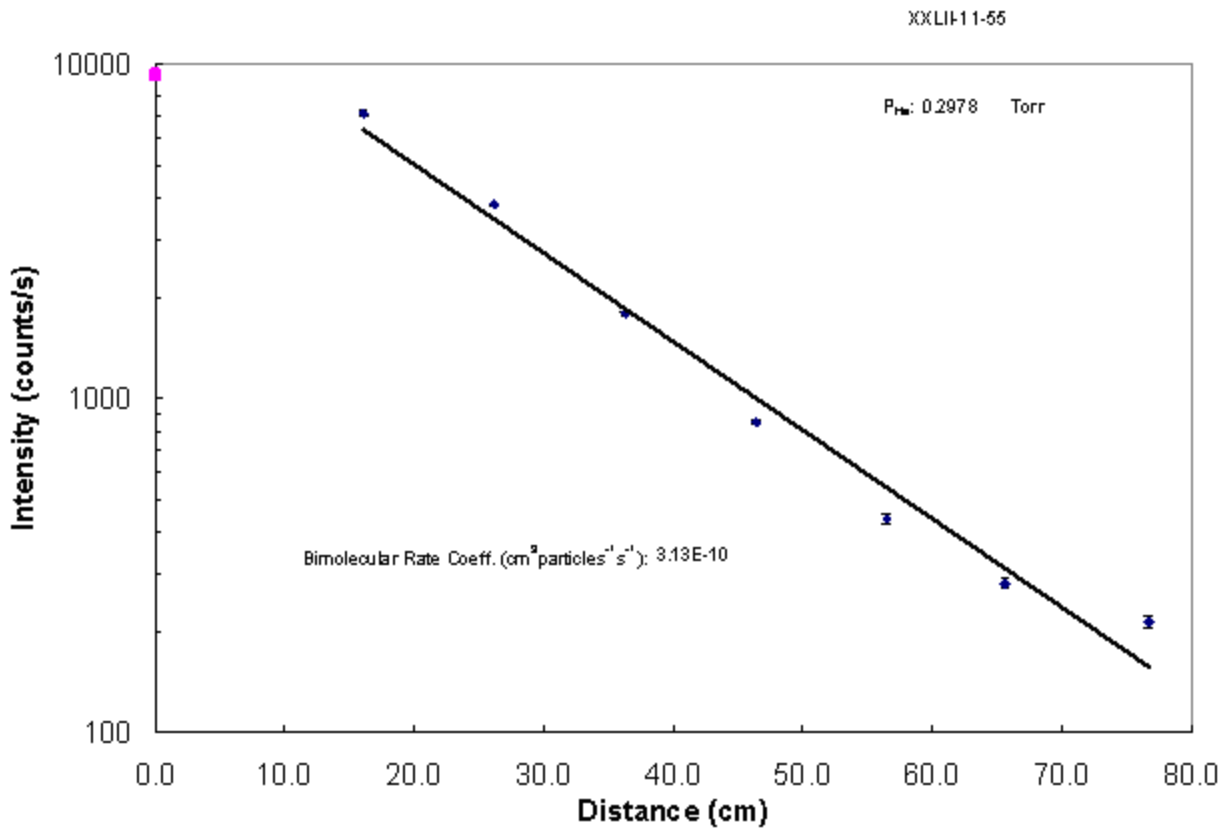

Figure 3.3 Kinetic Plot for the Reaction of $(Me_3Si)_2OMe^+$ with Ethyl Acetate

distribution. Figure 3.2 also reveals that no other ions are formed during the reaction of the trimethylsilyl cation and methoxytrimethylsilane.

The bis-trimethylsilylmethyloxonium ion was allowed to react with ethyl acetate to form the trimethylsilyl transfer product, $CH_3CO_2EtSiCH_3^+$ (equation 3.4). The reaction went to completion, had a rate constant of 3.50 (± 0.5) x 10^{-10} cm^3 $molecule^{-1}$ s^{-1}, and has an efficiency of 0.240. Figure 3.3 is a sample kinetic plot for the reaction of the bis-trimethylsilylmethyloxonium ion with ethyl acetate.

$$((CH_3)_3Si)_2OCH_3^+ \xrightarrow{CH_3CO_2Et} CH_3CO_2EtSi(CH_3)_3^+ + (CH_3)_3SiOCH_3 \qquad \textbf{3.4}$$

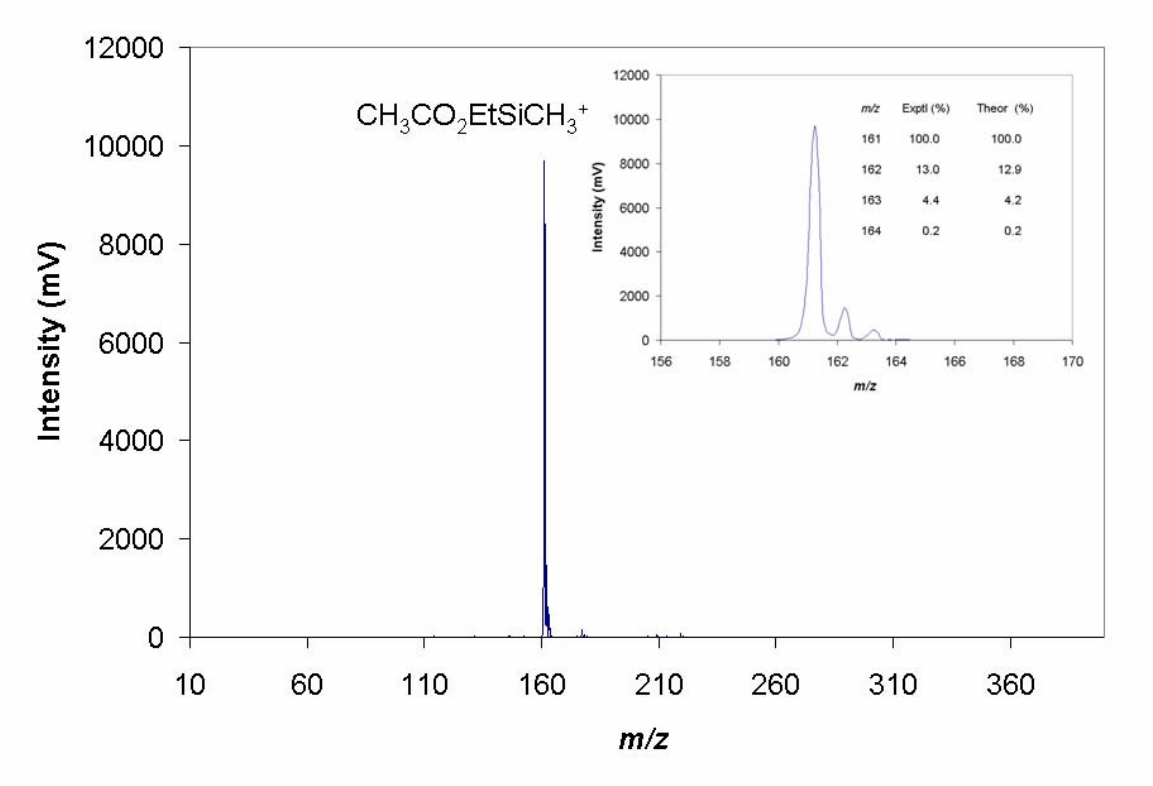

Figure 3.4 Trimethylsilyl Adduct of Ethyl Acetate Spectrum

Next, $((CH_3)_3Si)_2OCH_3^+$ was allowed to react with acetone (equation 3.5). Up to 2.2 Torr of acetone was added during this reaction. Trimethylsilyl transfer occurred; however, as depicted in equation 3.5, the reverse trimethylsilyl transfer from trimethylsilated acetone to methoxytrimethylsilane also occurred. Because these two reactions are in competition, the kinetics plot collected is curved and an accurate rate constant is unattainable.

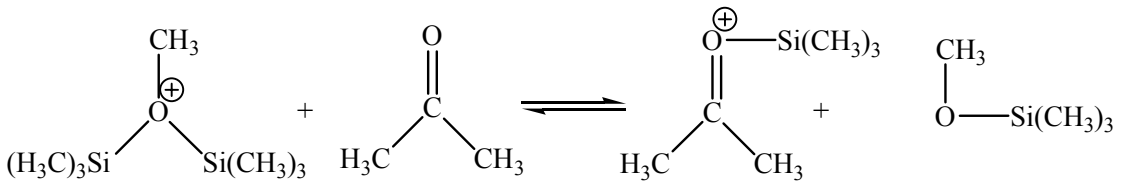

3.5

To support the supposition that the curved kinetics plots were due to the reverse reaction, two experiments were conducted. In the first, the bis-trimethylsilylmethyloxonium ion was allowed to react with acetone in the presence of varying pressures of methoxytrimethylsilane. Figure 3.5 is a series of kinetic plots showing the reaction rate dependence on the amount of methoxytrimethylsilane present. In the second reaction, the trimethylsilyl adduct of acetone, formed by allowing the trimethylsilyl cation to react with acetone, was allowed to react with methoxytrimethylsilane in the presence of different pressures of acetone. Figure 3.6 is a kinetic plot showing the reaction rate dependence on the amount of acetone present. Reactions with a constant rate are represented by a straight line on a kinetic plot. Both plots are curved and then level out at longer reaction distance, which suggests that reaction 3.5 is reaching a state of equilibrium independent of which direction the process is started from.

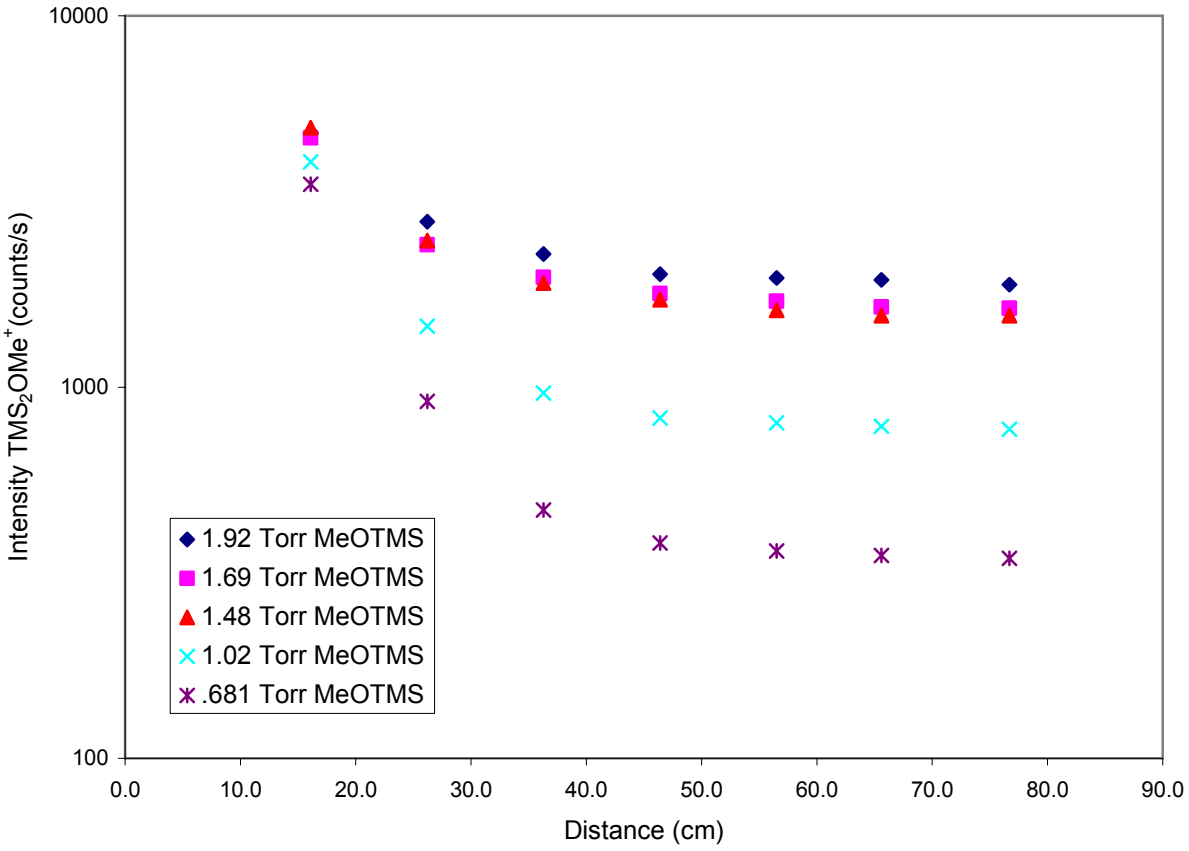

Figure 3.5 Kinetic Plot of the Reaction of Bis-trimethylsilylmethyloxonium Ion with Acetone

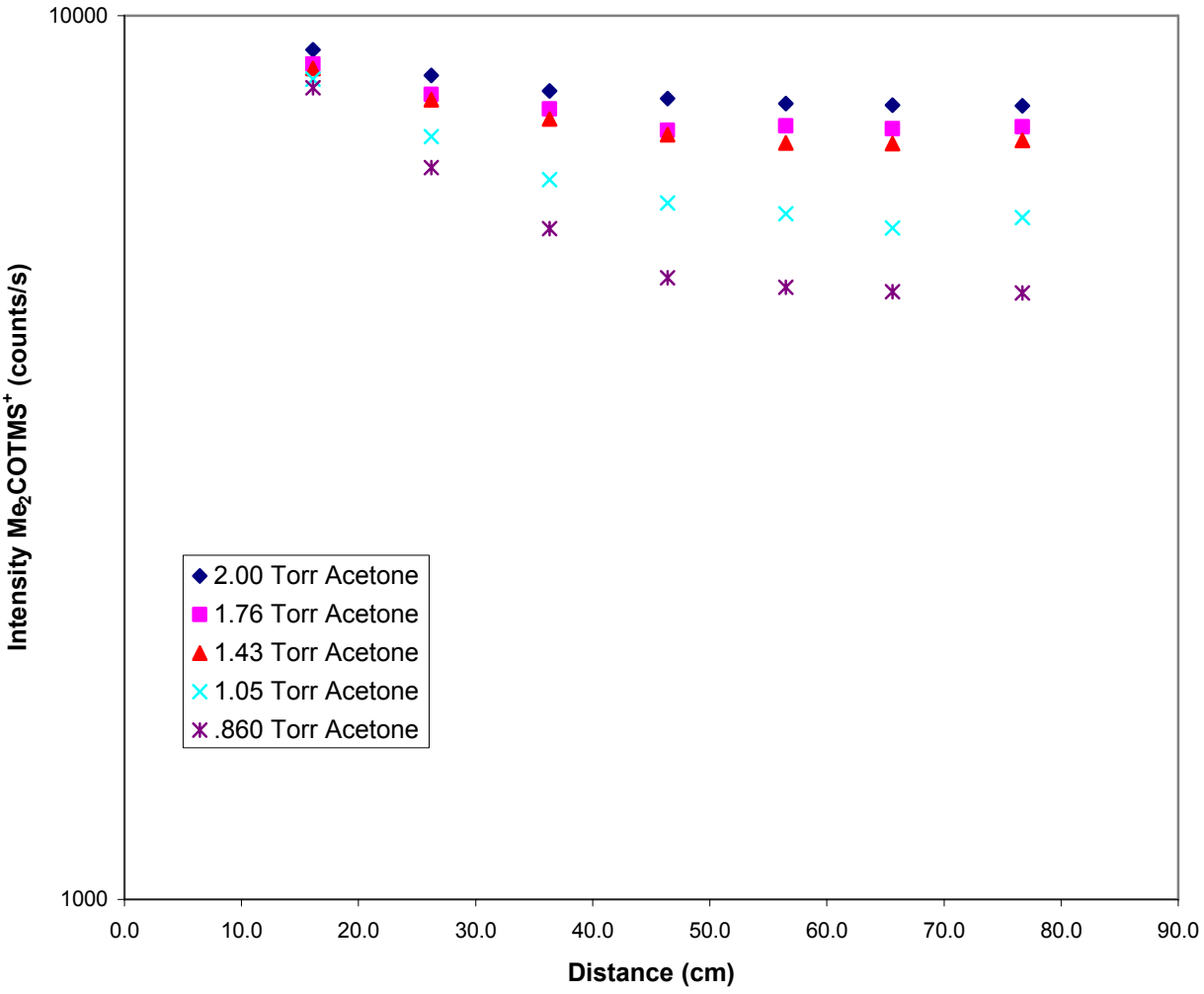

Figure 3.6 Kinetic Plot of the Reaction of the Me_2COTMS^+ with Methoxytrimethylsilane

The bis-trimethylsilylmethyloxonium ion was allowed to react with acetonitrile as shown in equation 3.6 to form the trimethylsilyl transfer product. This reaction did not go to completion even when up to 2.9 Torr of acetonitrile was added to the flow tube. The rate constant for this reaction was measured as 3.07 (± 8) x 10^{-12} cm^3 $molecule^{-1}$ s^{-1}, which corresponds to an efficiency of 0.001.

$$((CH_3)_3Si)_2OCH_3^+ \xrightarrow{CH_3CN} CH_3CNSi(CH_3)_3^+ + (CH_3)_3SiOCH_3 \qquad \textbf{3.6}$$

Both water and dimethylsulfide did not react with the bis-trimethylsilylmethyloxonium ion within the time window provided by the flowing afterglow. The limit obtained for the reaction with water was ≤ 9 x 10^{-12} cm^3 $molecule^{-1}$ s^{-1}, and the limit for the reaction of the bis-trimethylsilylmethyloxonium ion with dimethylsulfide was found to be ≤ 3 x 10^{-14} cm^3 $molecule^{-1}$ s^{-1}.

The products formed from the reaction of the bis-trimethylsilylmethyloxonium ion with triethylamine are protonated triethylamine, methylated triethylamine, and *m/z* 144. A hypothesized molecular formula for *m/z* 144 is $C_7H_{18}NSi^+$. An analysis of the isotopic distribution could not be performed because of the interference from $((CH_3)_3Si)_2^+$ at *m/z* 146. This ion was produced when tetramethylsilane was ionized. All of the products are primary products. Protonated and methylated triethylamine are the major products, and $C_7H_{18}NSi^+$ is a minor product. The rate constant for this reaction was determined to be 3.15 (± .002) x 10^{-12} cm^3 $molecule^{-1}$ s^{-1}, and the reaction had an efficiency of .003.

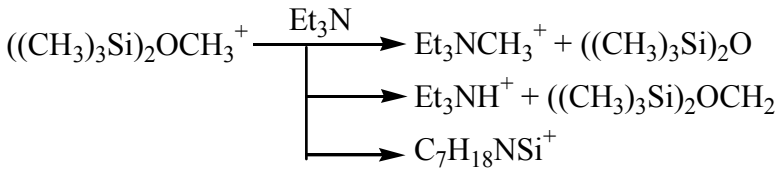

3.7

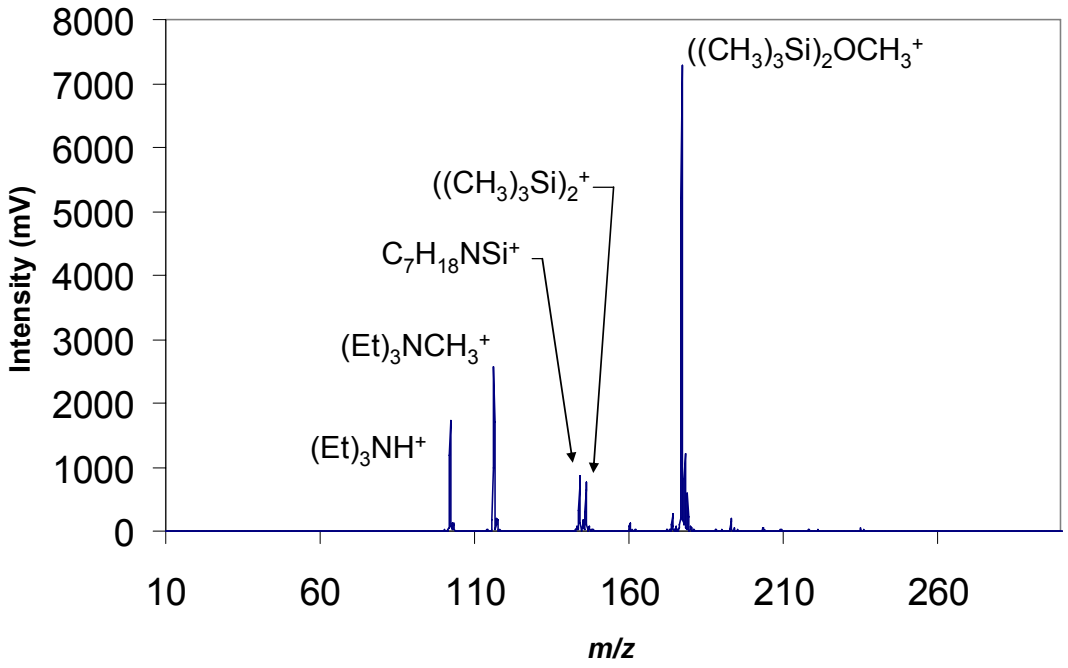

Figure 3.7 Spectrum of the Reaction of the Bis-trimethylsilylmethyloxonium Ion with Triethylamine

Table 3.1 Rate Constants for the Reaction of $(TMS)_2OCH_3^+$ with Selected Neutrals

Neutral	k_{obs} (Eff)[a]	Reaction
H_2O	≤ 0.009	No Reaction Obseved.
MeCN	0.00307 ± .008 (0.001)	100% TMST
MeCOMe		100% TMST
Me_2S	≤ 0.00003	No Reaction Obseved.
$MeCO_2CH_2Me$	0.350 ± .05 (0.240)	100% TMST
Et_3N	0.00315 ± .002 (0.003)	40% MeT, 40% E2, 20% Other

a—Units of 10^{-9} cm^3 $molecule^{-1}$ s^{-1}. Eff = k_{obs}/k_{coll}. k_{coll} is calculated via the VTST theory of Su and Bowers. (TMST – trimethylsilyl transfer, MeT – methyl transfer, PT – proton transfer)

3.4 DISCUSSION

For the reaction of the bis-trimethylsilylmethyloxonium ion with acetone, it is apparent that trimethylsilyl transfer is occurring from the trimethylsilyl adduct of acetone to methoxytrimethylsilane. This is supported by the curvature in the kinetic plots displayed in Figure 3.5, which shows that as the amount of methoxytrimethylsilane present is increased, the rate of reaction is decreased. For the reaction of the trimethylsilyl adduct of acetone with methoxytrimethylsilane shown in Figure 3.6, as the amount of acetone present was increased the apparent rate of that reaction decreased.

None of these neutrals show a reverse trimethylsilyl transfer reaction when allowed to react with protonated hexamethyldisiloxane. All of the rate constants for the reactions of the bis-trimethylsilylmethyloxonium ion are lower than the rate constants determined for protonated hexamethyldisiloxane with the same selected neutrals. For instance the rate constant for the reaction of protonated hexamethyldisiloxane with ethyl acetate has been recorded at 1.19 (± .01) x 10^{-9} cm^3 $molecule^{-1}$ s^{-1}, and the rate constant for the reaction of ethyl acetate with the bis-trimethylsilylmethyloxonium ion is 3.50 (± 0.5) x 10^{-10} cm^3 $molecule^{-1}$ s^{-1}. Both reactions occur by trimethylsilyl transfer. The differences in apparent rates between the reactions with protonated hexamethyldisiloxane and the bis-trimethylsilylmethyloxonium ion is likely an artifact due to the erroneous rates reported in this work due to the facile back reaction noted above.

3.5 CONCLUSIONS

The products of the initial reaction are altering the rate constants collected and causing the reaction rates to appear slow. Trimethylsilyl transfer was the primary reaction pathway, which bodes well for our goal of creating a novel reagent ion. The reaction system needs to be set up so that the back reaction does not occur and true rate constants can be obtained.

4.0 THE ATOMIC OXYGEN RADICAL ANION CHEMICAL IONIZATION PROCESS

4.1 INTRODUCTION

The need to understand the reactions taking place within our atmosphere lead to an interest in the chemistry of $O^{\cdot -}$.[21] Studies have focused on the role of $O^{\cdot -}$ in flames and the postulated role in plasmas.[22] Negative ion chemical ionization mass spectrometry and atmospheric pressure chemical ionization have utilized the $O^{\cdot -}$ as a reagent ion.[23] Specifically $O^{\cdot -}$ has been used to generate didehydro organic radical anions.[24] For instance, in equation 4.1 below, the cyanomethylene radical anion was readily synthesized from the reaction of $O^{\cdot -}$ with acetonitrile.[25] A similar reaction shown in equation 4.2 below was used to generate the tetramethyleneethane radical anion, $TME^{\cdot -}$, for a negative ion photoelectron spectroscopy study to determine the singlet-triplet gap of diradical tetramethyleneethane. In contrast to $TME^{\cdot -}$ being

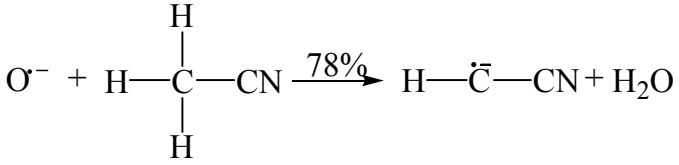

4.1

readily formed, a similar species, trimethylenemethane radical anion or $TMM^{\cdot -}$, is formed in very low yield via chemical ionization also shown in equation 4.3.[26]

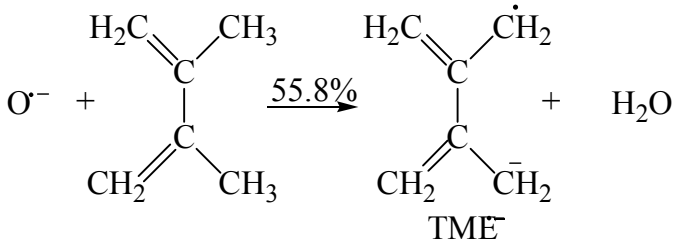

4.2

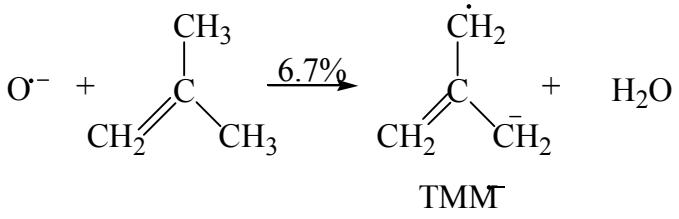

4.3

To gain a greater understanding of the reactions of $O^{\cdot -}$, a theoretical study of the reaction of $O^{\cdot -}$ with methanol was performed. This reaction was chosen because it involves a small number of heavy atoms and it has the possibility of competitive reaction channels. Experimental data has been published on the reaction of $O^{\cdot -}$ with methanol and various deuterated forms of methanol. The data collected by Futrell and Tiernan as well as Jager and coworkers suggests that hydrogen atom transfer is the dominant process.[27,28] Houriet and coworkers in an ICR study of the reaction found that proton transfer was the only process occurring.[29,30] The variation in these results was likely due to the varying experimental conditions. In the experiments by Futrell and Tiernan as well as Jager and coworkers $O^{\cdot -}$ had a higher energy than in the experiments by Houriet and coworkers. This added energy allowed a different portion of the potential surface to be sampled with the result that the product yields changed (with respect to Houriet's experiment).

4.2 COMPUTATIONAL METHODS

All calculations in this work were performed by my collaborator Dr. Gab-Yong Lee using the Gaussian 94 program.[31] The calculations used to create the potential energy surface (PES) for the reaction of $O^{\cdot-}$ with CH_3OH were carried out using density functional theory(DFT)[32,33] at Becke3LYP[34,35] level with the 6-31+G* basis set. As a form of method validation the gas phase acidities of MeOH, HO, and H_2O were calculated at 298K.

The equilibrium geometries and transition states for the all structures were fully optimized without any constraints. All calculations were performed with a self-consistent field convergence of 10^{-7} on the RMS density matrix and with 5D functions. At this level of theory, we have also calculated the harmonic vibrational frequencies to verify the nature of the corresponding true local minima or transition state, to provide the zero point vibrational energy (ZPE), and to obtain the thermodynamic contributions to the enthalpy.

Stationary points were characterized by the calculated Hessian matrix. Stable structures, corresponding to energy minima, were identified by possessing no negative eigenvalues of the Hessian, while transition states were identified by having one negative eigenvalue and one imaginary frequency. The identities of the transition state structures were verified by calculation of intrinsic reaction coordinates[36-38] (IRC) at this level of theory.

4.3 RESULTS

A reaction scheme and potential energy diagram for the possible products resulting from the reaction of the atomic oxygen radical anion with methanol was created. Scheme 4.1 shows three potential reaction pathways which would lead to the observable products: proton transfer from

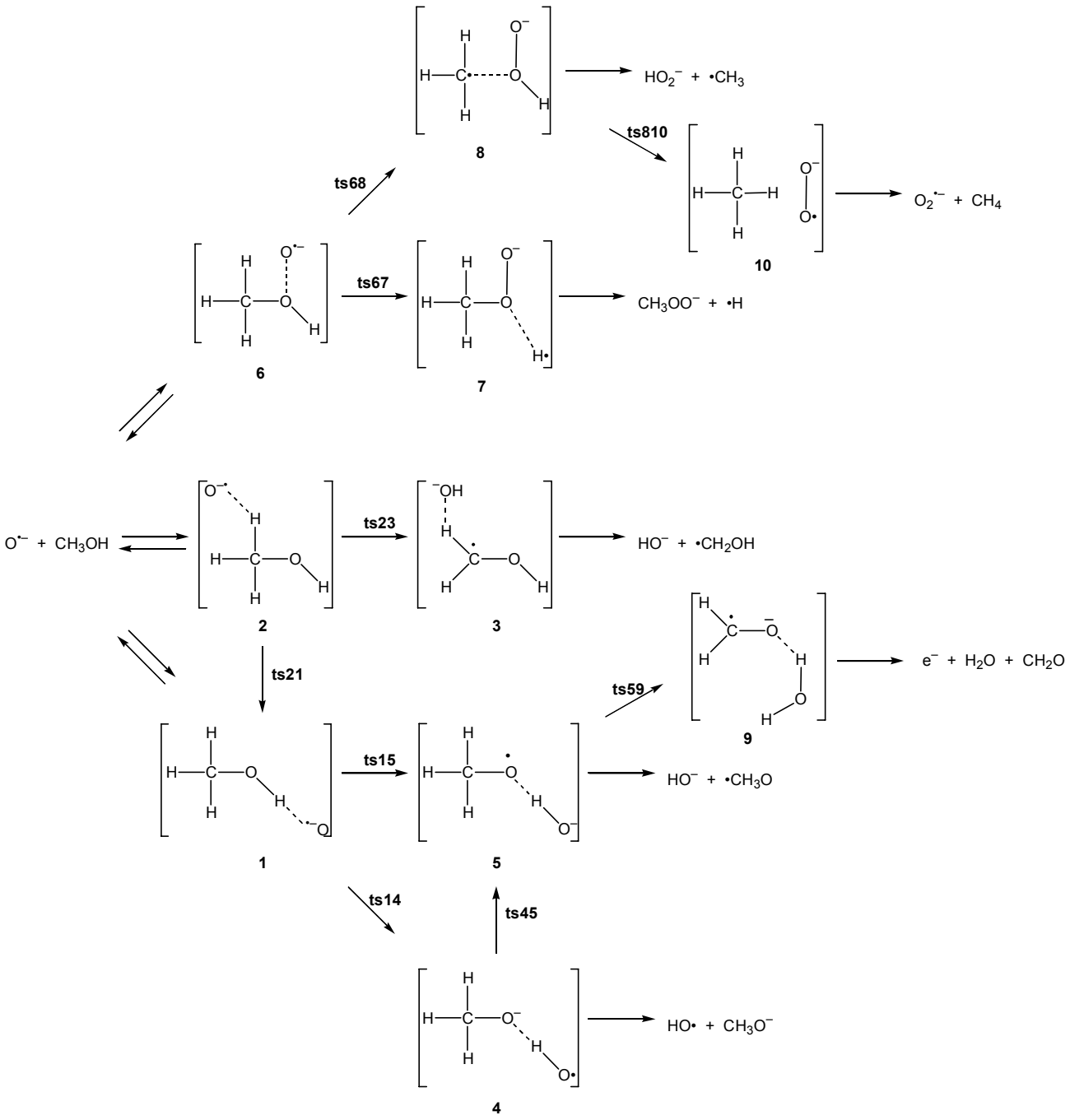

Scheme 4.1 Reaction Scheme for the Atomic Oxygen Radical Anion & Methanol

methanol's oxygen to yield hydroxide radical and methoxy anion, hydrogen atom transfer from methanol's carbon to yield hydroxide anion and the CH_2OH radical, and hydrogen atom transfer from methanol's oxygen to yield the hydroxide anion and methoxy radical. In addition, scheme 4.1 shows the formation of complex 6 leading to O-O containing products. The products from the pathways by which complex 6 might break down are not reported for a lack of the experimental data available to date. Scheme 4.1 also shows the reactive detachment pathway (complex 9) in which the products cannot be observed because they are uncharged. Optimizations were attempted to obtain data for complex 6, however, this complex was found to collapse to complex 1 in all studies performed. In Scheme 4.1 all species shown have been located and characterized by theory except for complex 5 and 6.

Table 4.2 contains the thermodynamic data used to create the potential energy diagram. On the potential energy diagram, Figure 4.1, line drawing structures are the authors imagination, while ball and stick structures are B3LYP/6-31+G* minimized entities. Likewise on Figure 4.1, numbers in parenthesis are experimental thermodynamic values and dashed lines are used to denote intermediates or transition states where no theoretical data has been found.

Table 4.1 Literature Data for the Reaction of $O^{\cdot-}$ with Methanol and Various Deuterated Forms of Methanol[27-30]

Neutral	k_{obs} (cm^3 $molecule^{-1}$ s^{-1})	Ion Product (observed and corresponding neutral)
CH_3OH	2.5×10^{-10}	67% HO^- + $CH_3O^{\cdot}$ 33% CH_3O^- + $HO^{\cdot}$
CH_3OH		75% HO^- + $CH_3O^{\cdot}$ 25% CH_3O^- + $HO^{\cdot}$
CH_3OD	2.0×10^{-10}	7% HO^- + $^{\cdot}CH_2OD$ 61% DO^- + $CH_3O^{\cdot}$ 32% CH_3O^- + $DO^{\cdot}$
CH_3OD		24% HO^- + $^{\cdot}CH_2OD$ 52% DO^- + $CH_3O^{\cdot}$ 25% CH_3O^- + $DO^{\cdot}$
CD_3OH	2.0×10^{-10}	65% HO^- + $CD_3O^{\cdot}$ 5% DO^- + $^{\cdot}CD_2OH$ 30% CD_3O^- + $HO^{\cdot}$
CD_3OD	1.7×10^{-10}	69% DO^- + $CD_3O^{\cdot}$ 31% CD_3O^- + $DO^{\cdot}$

Table 4.2 Heat of Formation Data for the Potential Energy Diagram

Name	$\Delta H_{f,(298K)}$ (a.u.)	$E_{(0K)}$ (a.u.)	Thermal Energy (a.u.)	$E_{(0K)}$ + Thermal Energy (a.u.)	$\Delta H_{f,(298)}$ (kcal/mol)
CH_3OO^-	-190.215717	-190.2616677	0.045950	-190.215718	49.0
$H\cdot$	-0.497912	-0.5002728	0.002360	-0.497913	
Complex 7	-190.723077	-190.7729112	0.049834	-190.723077	43.1
CH_3	-39.807970	-39.8418687	0.033898	-39.807971	35.4
HOO^-	-150.927319	-150.9440878	0.016769	-150.927319	
Complex 8	-190.743965	-190.7970427	0.053078	-190.743965	30.0
CH_3O^-	-115.070820	-115.1098256	0.039006	-115.070820	0.2
$HO^\cdot$	-75.720646	-75.7322173	0.011571	-75.720646	
CH_3OH	-115.667942	-115.7234888	0.055547	-115.667942	0.0
$O^{\cdot-}$	-75.123818	-75.1261784	0.002360	-75.123818	
ts23	-190.795951	-190.8447650	0.048814	-190.795951	-2.6
$CH_3O^\cdot$	-115.017130	-115.0576859	0.040556	-115.017130	-5.7
HO^-	-75.783752	-75.7953691	0.011617	-75.783752	
$^\cdot CH_2OH$	-115.019667	-115.0612052	0.041538	-115.019667	-7.3
HO^-	-75.783752	-75.7953691	0.011617	-75.783752	
Complex 2	-190.803539	-190.8607317	0.057193	-190.803539	-7.4
Complex 2	-190.803547	-190.8607315	0.057184	-190.803547	-7.4
CH_4	-40.471084	-40.5198904	0.048807	-40.471083	-12.9
O_2^-	-150.341177	-150.3471683	0.005992	-150.341176	
ts9	-190.814668	-190.8641261	0.049459	-190.814667	-14.4
Complex 3	-190.815969	-190.8701474	0.054178	-190.815969	-15.2
Complex 10	-190.817146	-190.8730449	0.055899	-190.817146	-15.9
ts14	-190.838332	-190.8931330	0.054801	-190.838332	-29.2
Complex 1	-190.841925	-190.8955589	0.053634	-190.841925	-31.5
Complex 4	-190.844336	-190.8966019	0.052266	-190.844336	-33.0
Complex 4	-190.844337	-190.8966068	0.052270	-190.844337	-33.0
H_2CO^-	-114.456939	-114.4841815	0.027243	-114.456938	-38.6
H_2O	-76.396387	-76.4212203	0.024834	-76.396386	
$H_2C{=}O$	-114.476511	-114.5070884	0.030577	-114.476511	-50.9
H_2O	-76.396387	-76.4212203	0.024834	-76.396386	
Complex 9	-190.883103	-190.9376636	0.054560	-190.883104	-57.3

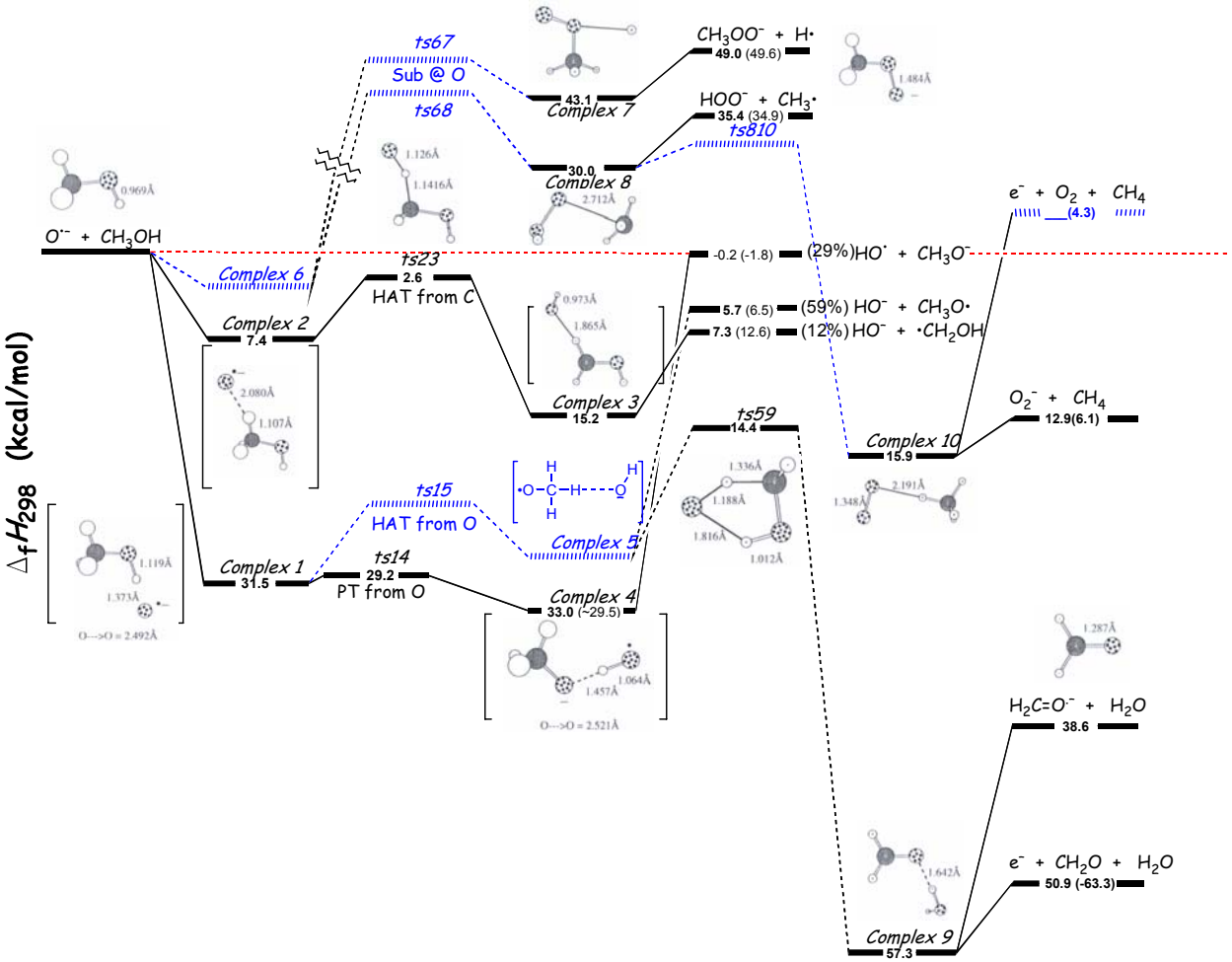

Figure 4.1 Potential Energy Diagram for the Reaction of $O^{\bullet-}$ with Methanol

4.4 DISCUSSION

Houriet and coworkers data shows that proton transfer is the only process occurring under their experimental conditions. This correlates with the potential energy diagram provided by the theoretical study.[29,30] Proton transfer is the favored pathway because the formation of complex 1 is more energetically favorable than complex 2 or 6 and because there is a smaller activation barrier for proton transfer versus hydrogen atom transfer from methanol's oxygen. The reactive detachment pathway might be expected to produce the next greatest amount of product because it has a smaller activation barrier than forming the hydrogen atom transfer from methanol's oxygen products. Experimentally the products from this channel can not be observed since none have a charge. This leaves the hydrogen atom transfer from methanol's carbon to produce the least amount of product. Therefore, the potential energy surface computed during this study suggests that at 298 K the expected product distribution would be only proton transfer, consistent with Houriet's observations.

The data provided by Futrell and Tiernan as well as Jager, Henglein, and Simic in Table 4.1 shows that hydrogen atom transfer from methanol's oxygen is favored at 67% and 75%.[27,28] Because hydrogen abstraction has a higher activation barrier than proton transfer from methanol's oxygen, it would be expected that proton transfer would be the dominant process. It is likely that the conditions used during these latter experiments provide extra energy needed to the system in order to access a different portion of the potential energy surface.

Other products from the pathway beginning with complex 6 are not seen because complex 1 and 2 are more energetically favorable, there is a large energy barrier to overcome in

order to form transition state 67 and 68, and all of the products resulting from these pathways except for one are endothermic.

4.5 CONCLUSIONS

The potential energy surface computed during this study would suggest that at 298 K the expected product distribution would be only proton transfer.

APPENDIX A

KINETIC DATA FOR THE REACTIONS OF THE BIS-TRIMETHYLSILYLMETHYLOXONIUM ION

RXN = $(TMS)_2OCH_3^+$ + ethyl acetate

Data	XXLII-11-55	XXLII-11-55A	XXLII-11-55B	XXLII-11-56	XXLII-11-56A
Date (data collected)	9/22/2005	9/22/2005	9/22/2005	9/24/2005	9/24/2005
P(He)	0.2978	0.2984	0.2988	0.3701	0.3719
P(He) err	0.0004	0.0003	0.0001	0.0013	0.0006
P(He) err %	0.1%	0.1%	0.0%	0.4%	0.2%
F(He) (STP cc/s)	105.51	105.51	105.51	148.89	148.89
F(He) err	0.00	0.00	0.00	0.00	0.00
F(He) err %	0.0%	0.0%	0.0%	0.0%	0.0%
He calib:	4/27/1992	4/27/1992	4/27/1992	4/27/1992	4/27/1992
Quench Gas?	No	No	No	No	No
T	299.1	299.1	299.1	298.1	298.1
Pvr (Port min)	0.739	0.728	0.758	0.836	0.856
Pvr (Port max)	0.769	0.767	0.802	0.879	0.881
k	3.13E-10	3.18E-10	3.15E-10	3.95E-10	4.10E-10
m-err (%)	5.7%	6.0%	6.2%	3.8%	3.9%
R	0.9904	0.9893	0.9886	0.9956	0.9954
F(neut)	2.41E-02	2.37E-02	2.40E-02	2.44E-02	2.36E-02
F(neut) err	7.11E-04	6.35E-04	5.49E-04	1.60E-04	1.02E-03
F(neut) err %	3.0%	2.7%	2.3%	0.7%	4.3%
Vac Rack used	bottom arm, w/bulb	bottom arm, w/bulb	bottom arm, w/bulb	bottom arm, w/bulb	bottom arm, w/bulb
Vac Rack calib	10/6/2004	10/6/2004	10/6/2004	10/6/2004	10/6/2004
z	Varies	Varies	Varies	Varies	Varies
falloff	33.1	34.4	35.56	27.56	30.30
# of half-lives	5.05	5.11	5.15	4.78	4.92
Plot quality					
Comments					

k = 3.50E-10
std dev = 4.80697E-11
std dev (%) = 13.7%
Count = 5

alpha = 8.62E-24 **Source =** CRC 2000 Elect
dipole = 1.78 ± .09 **Source =** CRC 2000 Elect

k(ADO) = 1.26E-09 **Eff(ADO) =** 27.9%

k(SC) = 1.46E-09 **Eff(SC) =** 24.0%

Kinetic Plots for the Reaction of Bis-Trimethylsilylmethyloxonium Ion with Ethyl Acetate

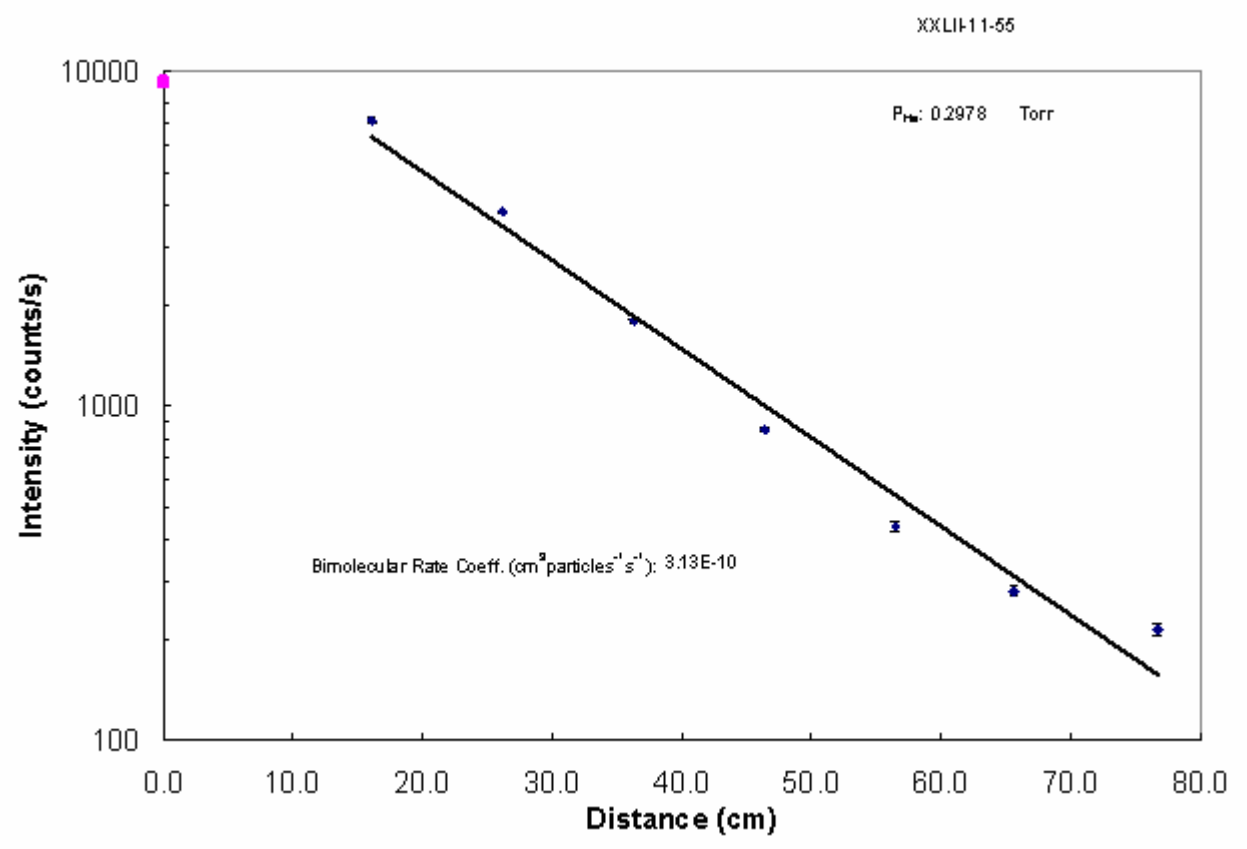

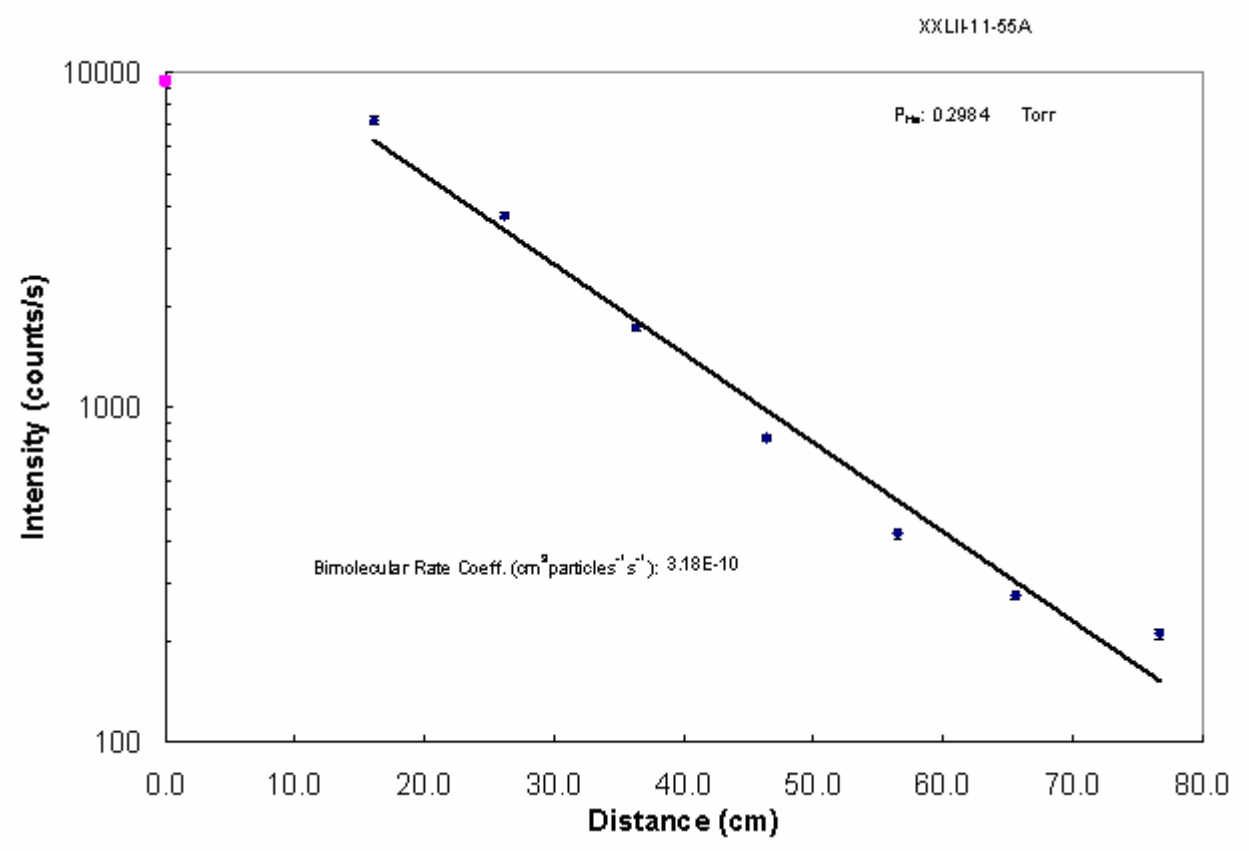
XXLII-11-55A
P_{He}: 0.2984 Torr
Bimolecular Rate Coeff. ($cm^3 particles^{-1} s^{-1}$): 3.18E-10
Intensity (counts/s)
Distance (cm)
10000
1000
100
0.0
10.0
20.0
30.0
40.0
50.0
60.0
70.0
80.0

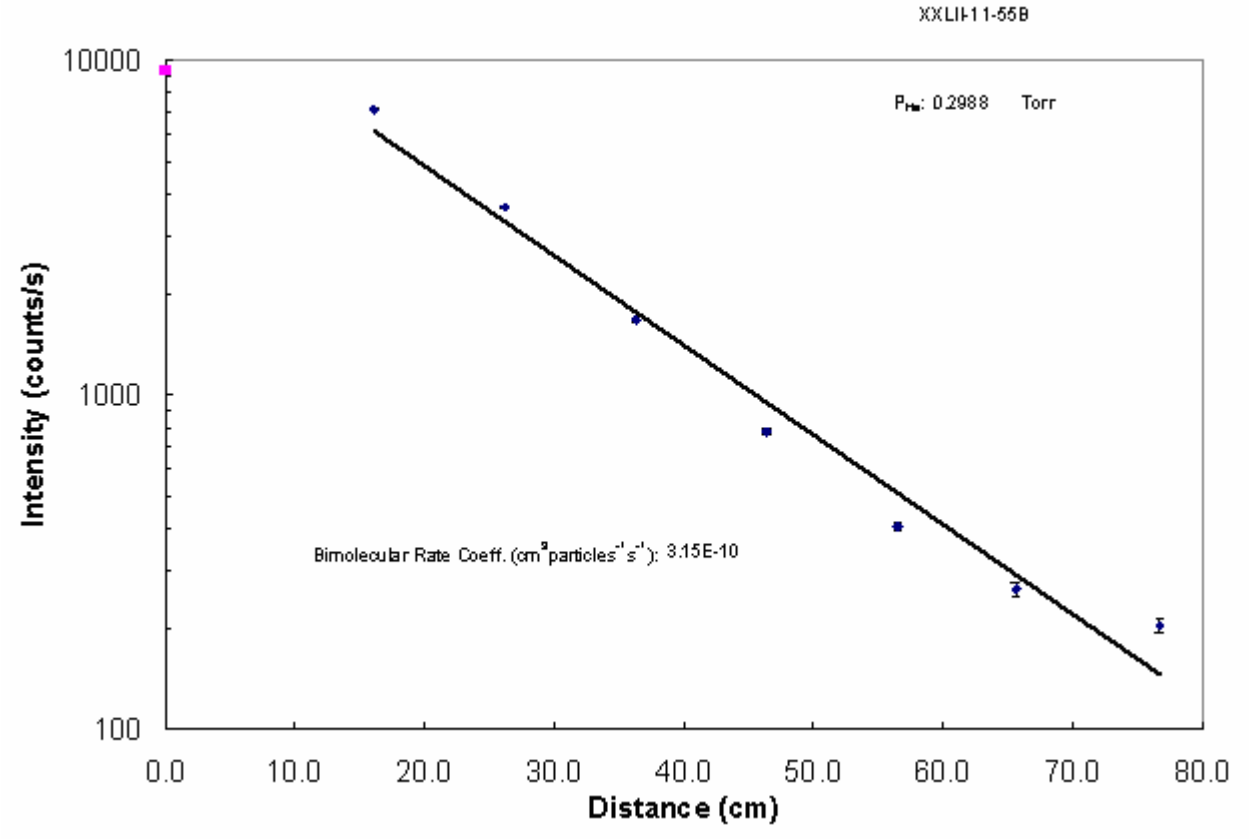
XXLII-11-55B
P_{He}: 0.2988 Torr
Bimolecular Rate Coeff. ($cm^3 particles^{-1} s^{-1}$): 3.15E-10
Intensity (counts/s)
Distance (cm)
10000
1000
100
0.0
10.0
20.0
30.0
40.0
50.0
60.0
70.0
80.0

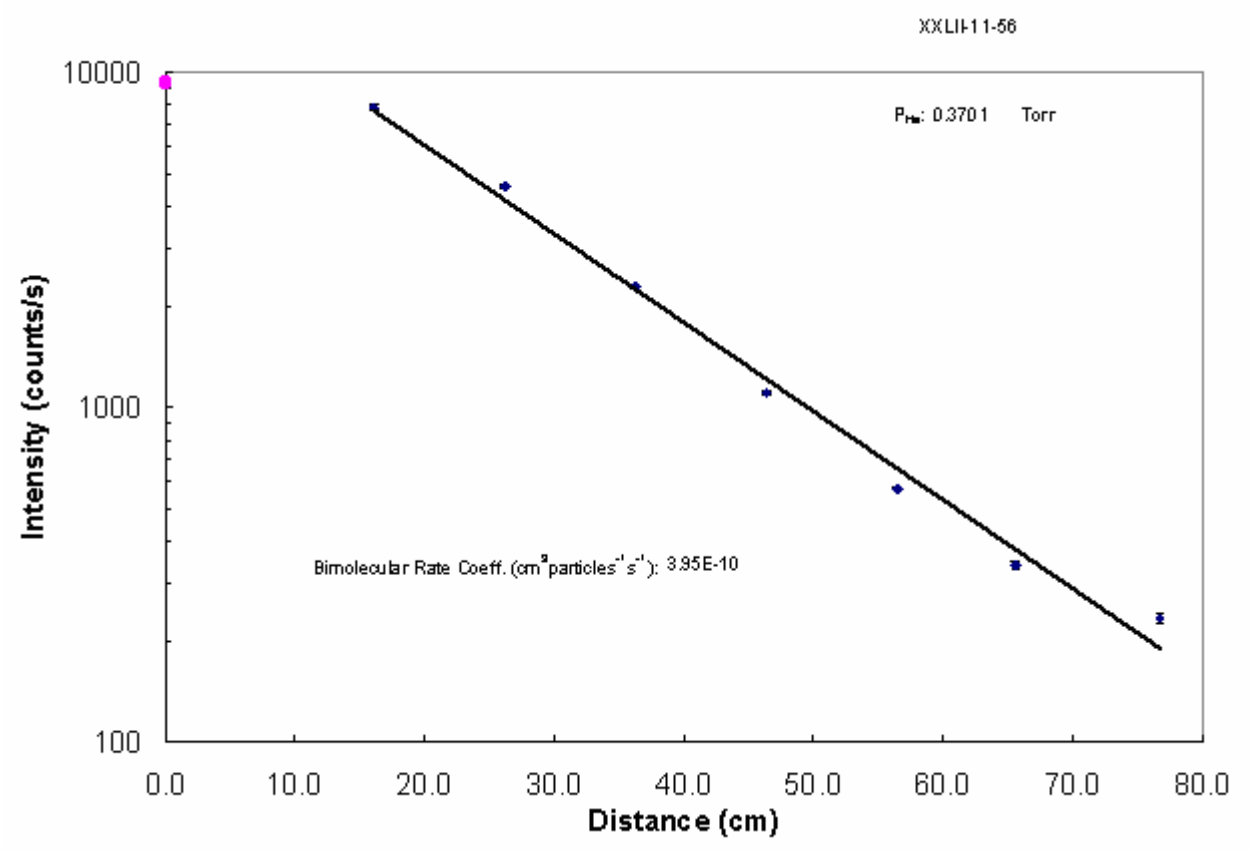
XXLII-11-56
P_{He}: 0.3701 Torr
Bimolecular Rate Coeff. ($cm^3 particles^{-1} s^{-1}$): 3.95E-10
Intensity (counts/s)
Distance (cm)
10000
1000
100
0.0
10.0
20.0
30.0
40.0
50.0
60.0
70.0
80.0

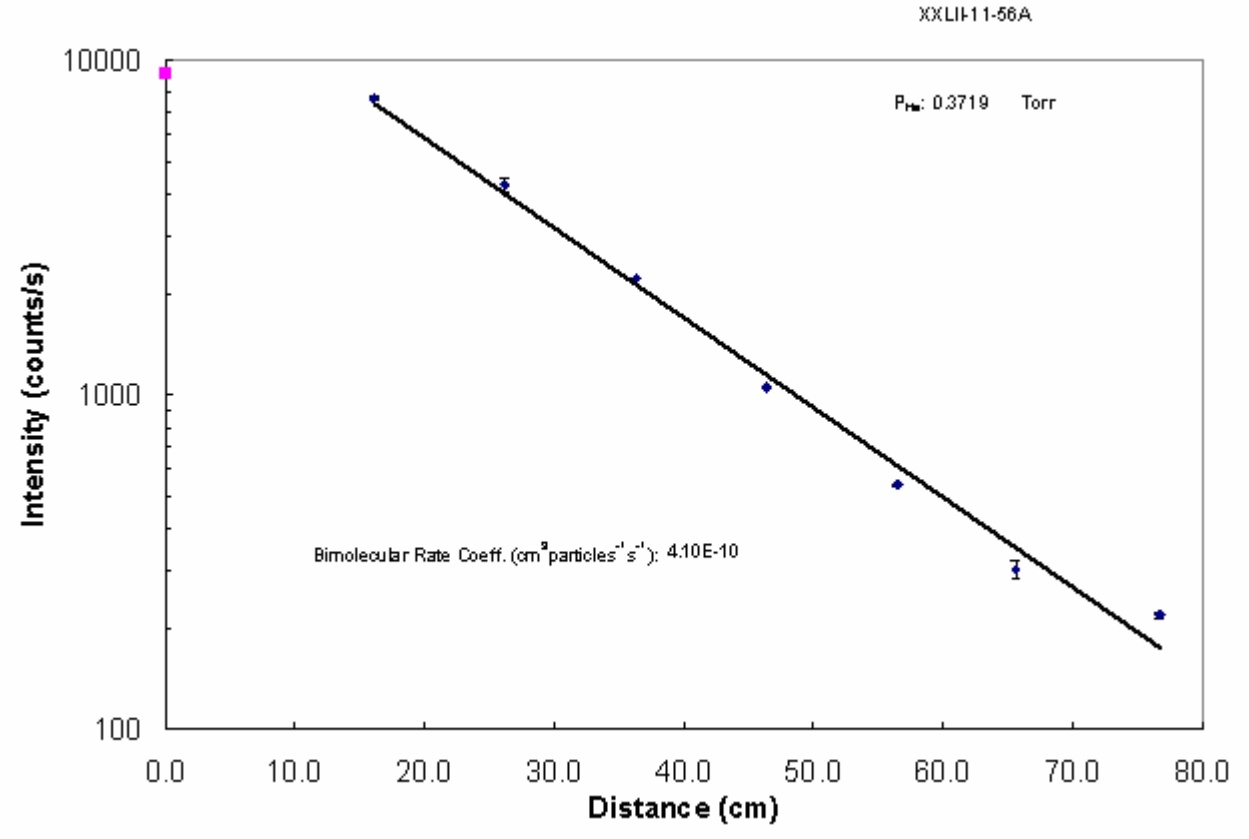
XXLII-11-56A
P_{He}: 0.3719 Torr
Bimolecular Rate Coeff. ($cm^3 particles^{-1} s^{-1}$): 4.10E-10
Intensity (counts/s)
Distance (cm)
10000
1000
100
0.0
10.0
20.0
30.0
40.0
50.0
60.0
70.0
80.0

RXN = $(TMS)_2OCH_3^+$ + Acetonitrile

Data	XXLII-11-52	XXLII-11-52A	XXLII-11-54	XXLII-11-54B	XXLII-11-54C
Date (data collected)	9/15/2005	9/15/2005	9/22/2005	9/22/2005	9/22/2005
P(He)	0.3252	0.3262	0.4232	0.4268	0.4279
P(He) err	0.0005	0.0005	0.0008	0.0004	0.0006
P(He) err %	0.2%	0.2%	0.2%	0.1%	0.1%
F(He) (STP cc/s)	120.87	120.87	168.5	168.50	168.50
F(He) err	0.00	0.00	0.00	0.00	0.00
F(He) err %	0.0%	0.0%	0.0%	0.0%	0.0%
He calib:	4/27/1992	4/27/1992	4/27/1992	4/27/1992	4/27/1992
Quench Gas?	No	No	No	No	No
T	300.1	300.1	299.1	299.1	299.1
Pvr (Port min)			1.876	1.795	1.872
Pvr (Port max)			2.028	1.939	1.998
k	2.29E-12	2.09E-12	3.57E-12	3.88E-12	3.50E-12
m-err (%)	8.6%	5.4%	16.6%	24.9%	22.6%
R	0.9785	0.9913	0.9265	0.8540	0.8744
F(neut)	1.93E-01	1.84E-01	1.59E-01	1.63E-01	1.57E-01
F(neut) err	4.81E-03	1.18E-03	8.20E-03	7.86E-04	7.79E-04
F(neut) err %	2.5%	0.6%	5.2%	0.5%	0.5%
Vac Rack used	bottom arm, w/bulb	bottom arm, w/bulb	bottom arm, w/bulb	bottom arm, w/bulb	bottom arm, w/bulb
Vac Rack calib	10/6/2004	10/6/2004	10/6/2004	10/6/2004	10/6/2004
z	Varies	Varies	Varies	Varies	Varies
falloff	1.3	1.3	1.33	1.37	1.38
# of half-lives	0.36	0.35	0.41	0.45	0.46
Plot quality					
Comments					

k = 3.07E-12
std dev = 8.15432E-13
std dev (%) = 26.6%
Count = 5

alpha = 4.48E-24 **Source =** CRC 2000 Elect
dipole = 3.92519 **Source =** CRC 2000 Elect

k(ADO) = 8.59E-10 **Eff(ADO) =** 0.4%

k(SC) = 3.18E-09 **Eff(SC) =** 0.1%

Kinetic Plots for the Reaction of the Bis-trimethylsilylmethyloxonium Ion and Acetonitrile

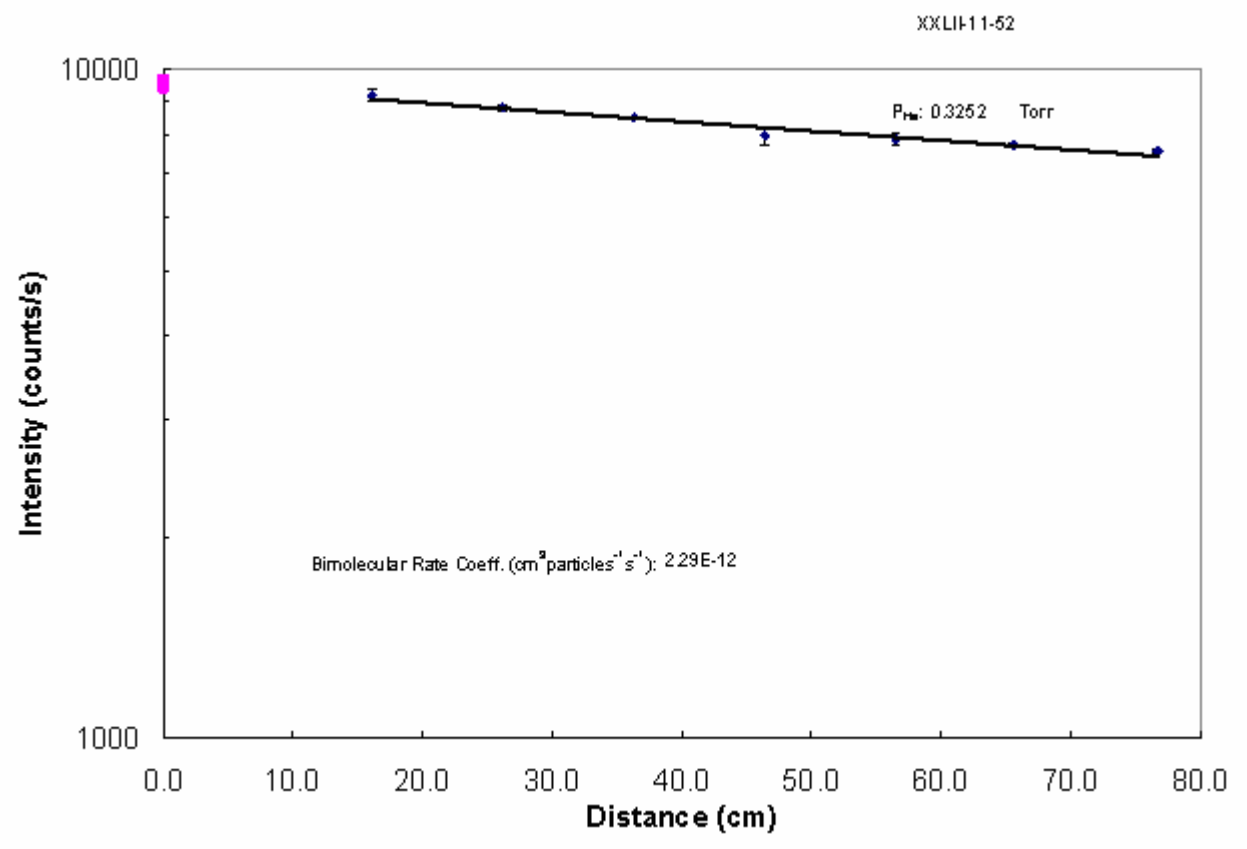

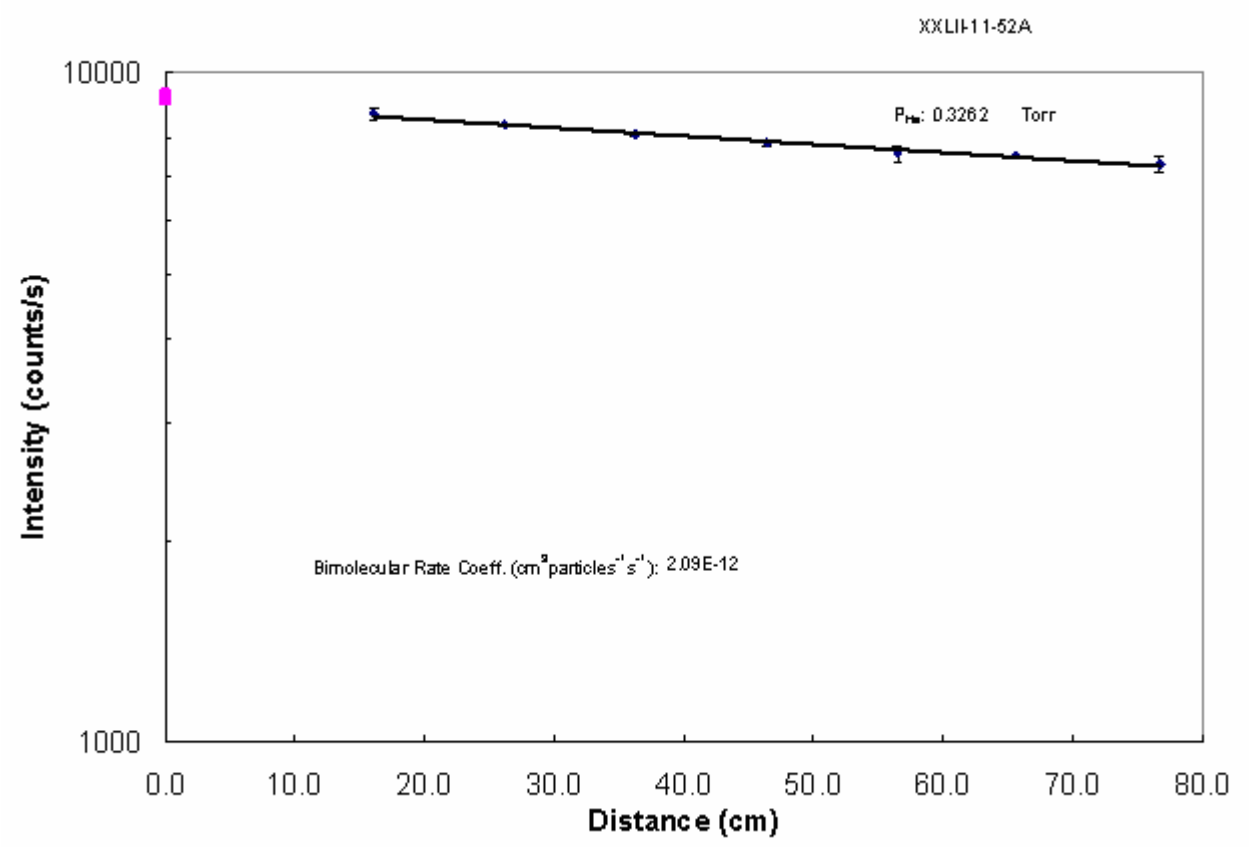
XXLII-11-52A
10000
1000
P_{He}: 0.3262 Torr
Bimolecular Rate Coeff. ($cm^3 particles^{-1} s^{-1}$): 2.09E-12
Intensity (counts/s)
0.0
10.0
20.0
30.0
40.0
50.0
60.0
70.0
80.0
Distance (cm)

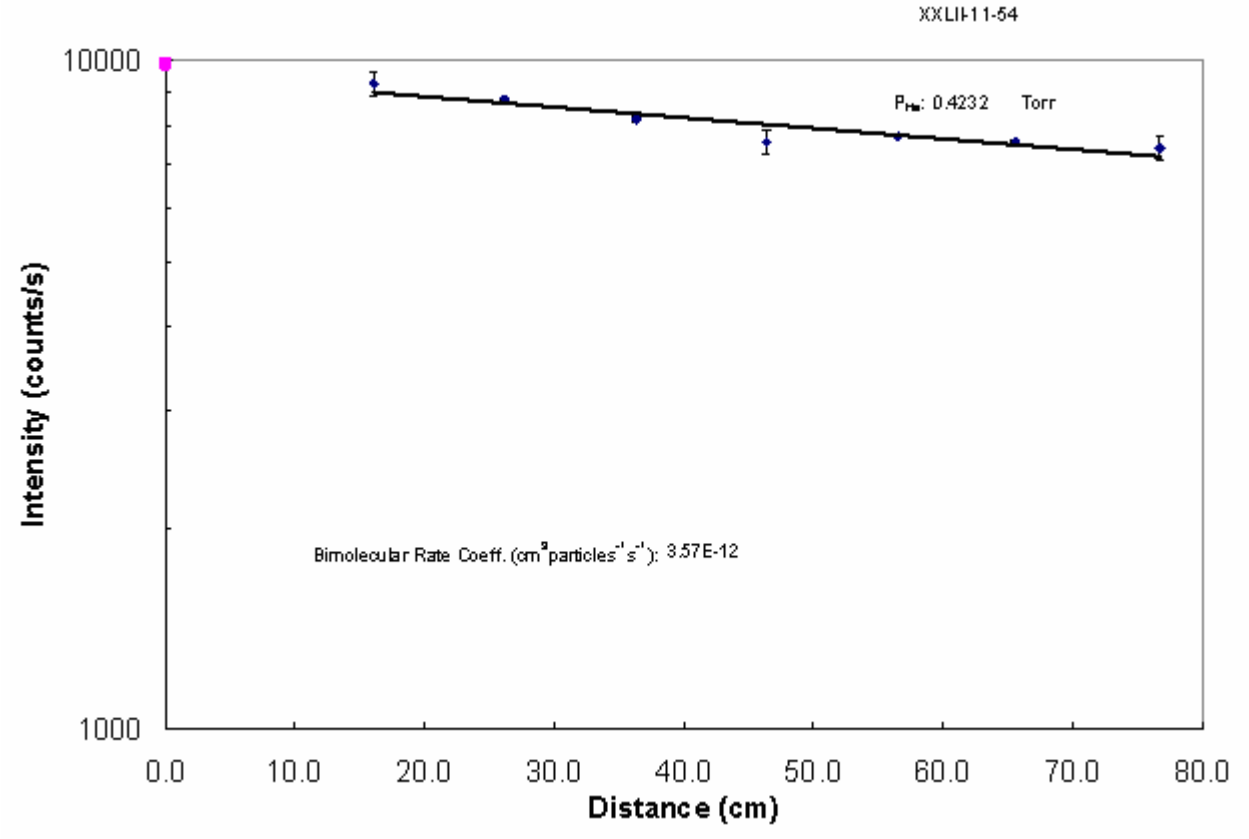
XXLII-11-54
10000
1000
P_{He}: 0.4232 Torr
Bimolecular Rate Coeff. ($cm^3 particles^{-1} s^{-1}$): 3.57E-12
Intensity (counts/s)
0.0
10.0
20.0
30.0
40.0
50.0
60.0
70.0
80.0
Distance (cm)

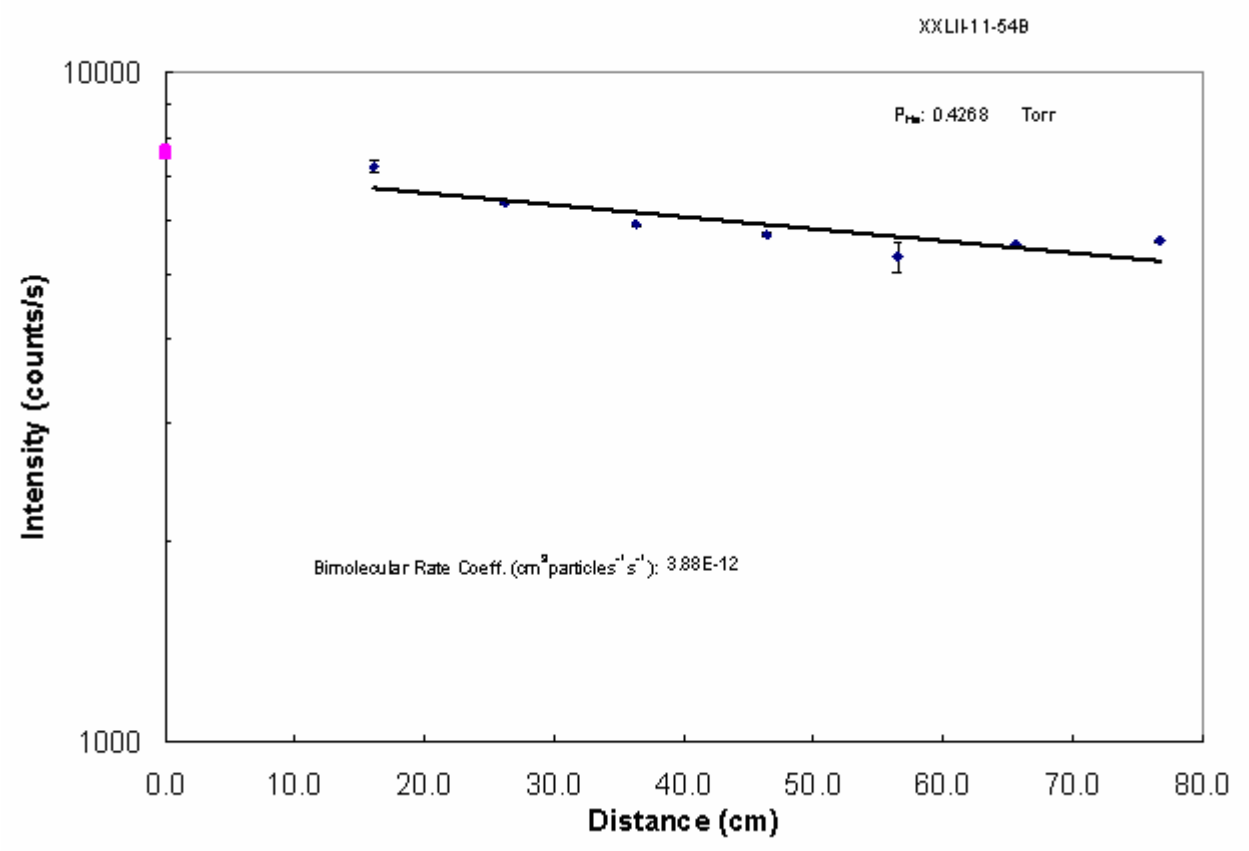
XXLII-11-54B
10000
1000
P_{He}: 0.4268 Torr
Intensity (counts/s)
Bimolecular Rate Coeff. ($cm^3 particles^{-1} s^{-1}$): 3.88E-12
0.0
10.0
20.0
30.0
40.0
50.0
60.0
70.0
80.0
Distance (cm)

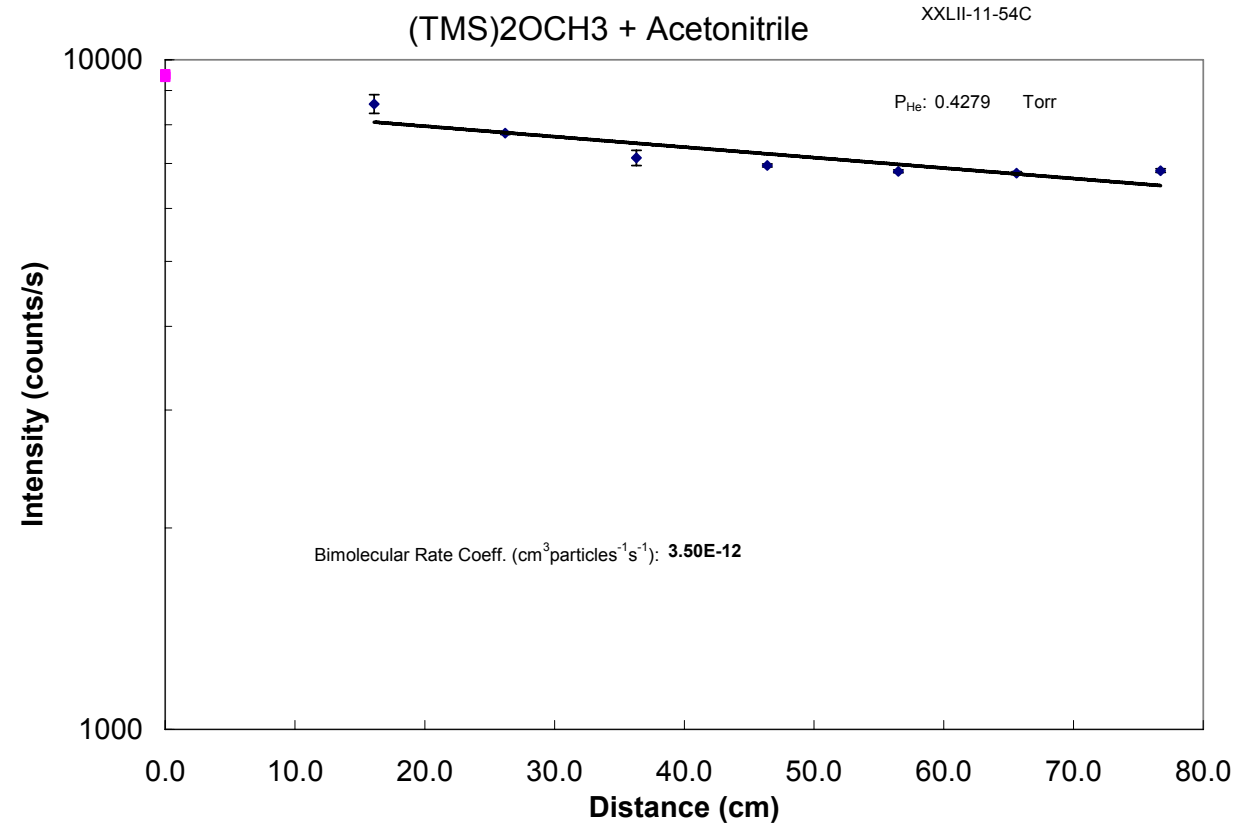
(TMS)2OCH3 + Acetonitrile
XXLII-11-54C
10000
1000
P_{He}: 0.4279 Torr
Intensity (counts/s)
Bimolecular Rate Coeff. ($cm^3 particles^{-1} s^{-1}$): 3.50E-12
0.0
10.0
20.0
30.0
40.0
50.0
60.0
70.0
80.0
Distance (cm)

RXN =	$(TMS)_2OCH_3^+ + H_2O$
Data	XXLII-11-49
Date (data collected)	9/8/2005
P(He)	0.3257
P(He) err	0.001
P(He) err %	0.3%
F(He) (STP cc/s)	121.04
F(He) err	0.00
F(He) err %	0.0%
He calib:	4/27/1992
Quench Gas?	No
T	299.1
Pvr (Port min)	
Pvr (Port max)	
k	9.05E-13
m-err (%)	28.9%
R	0.8157
F(neut)	1.50E-01
F(neut) err	3.55E-03
F(neut) err %	2.4%
Vac Rack used	bottom arm, w/bulb
Vac Rack calib	10/6/2004
z	Varies
falloff	1.1
# of half-lives	0.12
Plot quality	
Comments	

k =	9.05E-13		
std dev =			
std dev (%) =			
Count =	1		
alpha =	1.45E-24	**Source =**	CRC 2000 Elect
dipole =	1.8546 ± 0.0040	**Source =**	CRC 2000 Elect
k(ADO) =	1.75E-09	**Eff(ADO) =**	0.1%
k(SC) =	2.22E-09	**Eff(SC) =**	0.0%

Kinetic Plot for the Reaction of the Bis-trimethylsilylmethyloxonium Ion and Water

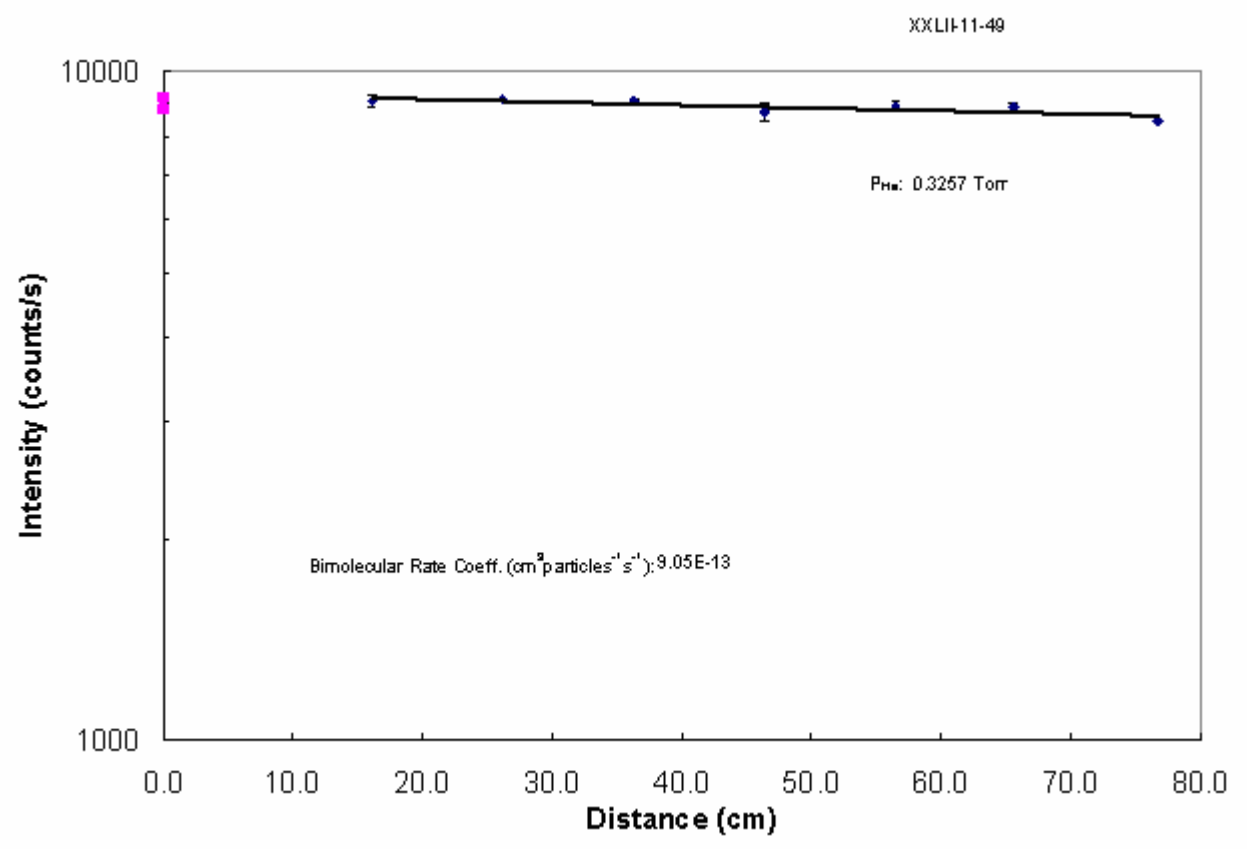

RXN =	$(TMS)_2OCH_3^+ + Me_2S$
Data	XXLII-11-59D
Date (data collected)	10/5/2005
P(He)	0.3457
P(He) err	0.0001
P(He) err %	0.0%
F(He) (STP cc/s)	131.67
F(He) err	0.00
F(He) err %	0.0%
He calib:	4/27/1992
Quench Gas?	No
T	298.4
Pvr (Port min)	1.750
Pvr (Port max)	1.899
k	2.79E-14
m-err (%)	484.6%
R	0.1026
F(neut)	9.62E-02
F(neut) err	3.83E-04
F(neut) err %	0.4%
Vac Rack used	bottom arm, w/bulb
Vac Rack calib	10/6/2004
z	Varies
falloff	
# of half-lives	
Plot quality	
Comments	

k =	2.79E-14		
std dev =			
std dev (%) =			
Count =	1		
alpha =	7.41E-24	**Source =**	CRC 2000 Elect
dipole =	1.554 ± .004	**Source =**	CRC 2000 Elect
k(ADO) =	1.29E-09	**Eff(ADO) =**	0.0%
k(SC) =	1.48E-09	**Eff(SC) =**	0.0%

Kinetic Plot for the Reaction of the Bis-trimethylsilylmethyloxonium Ion and Dimethyl Sulfide

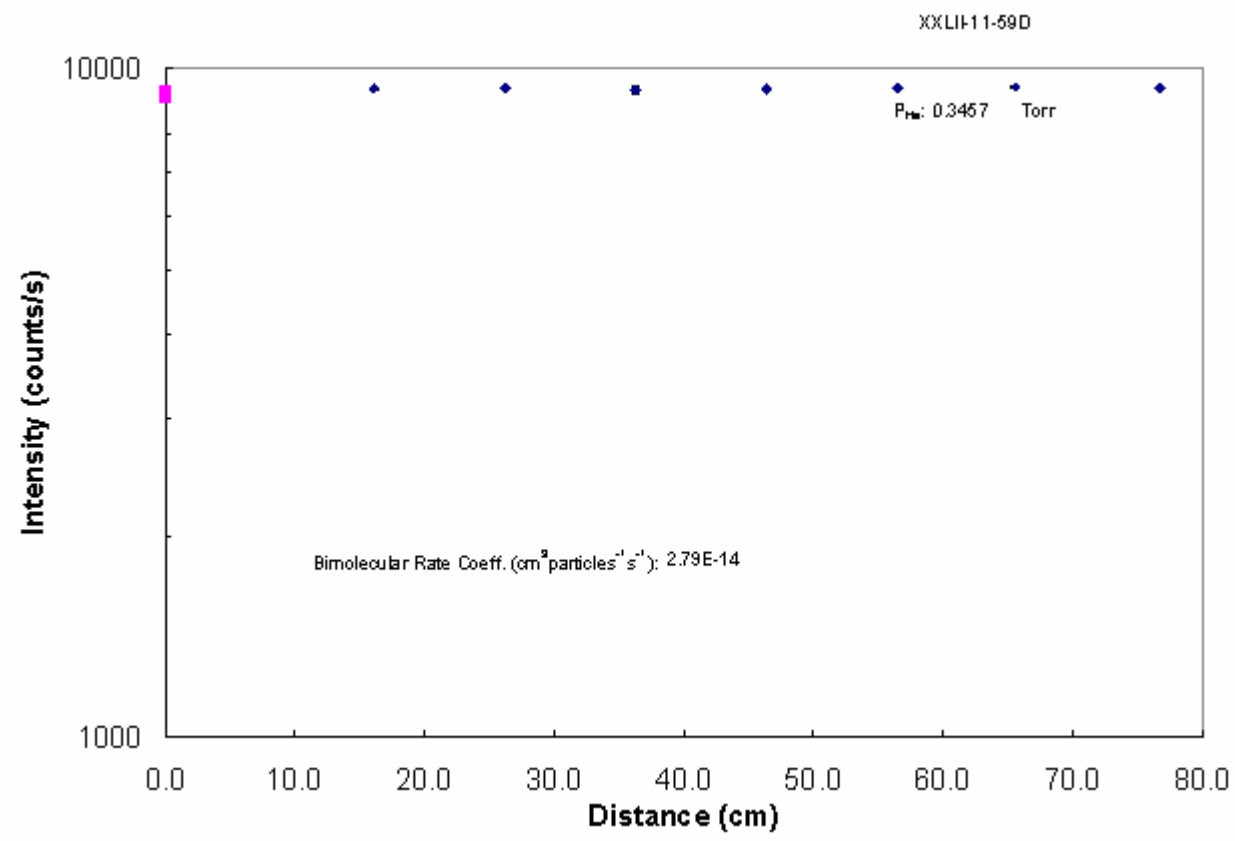

RXN = $(TMS)_2OCH_3^+ + Et_3N$

Data	XLII-11-51	XLII-11-51A	XLII-11-51B	XLII-11-59B	XLII-11-59C
Date (data collected)	9/12/2005	9/12/2005	9/12/2005	10/5/2005	10/5/2005
P(He)	0.331	0.3314	0.3317	0.359	0.3593
P(He) err	0.0002	0.0001	0.0001	0.0001	0.0002
P(He) err %	0.1%	0.0%	0.0%	0.0%	0.1%
F(He) (STP cc/s)	122.73	122.73	122.73	138.42	138.42
F(He) err	0.00	0.00	0.00	0.00	0.00
F(He) err %	0.0%	0.0%	0.0%	0.0%	0.0%
He calib:	4/27/1992	4/27/1992	4/27/1992	4/27/1992	4/27/1992
Quench Gas?	No	No	No	No	No
T	298.4	298.4	298.4	298.4	298.4
Pvr (Port min)				2.011	2.063
Pvr (Port max)				2.171	2.228
k	4.54E-12	4.46E-12	4.35E-12	1.09E-12	1.31E-12
m-err (%)	6.8%	5.4%	3.8%	18.1%	41.3%
R	0.9863	0.9915	0.9964	0.9145	0.7028
F(neut)	1.26E-01	1.24E-01	1.21E-01	9.59E-02	9.60E-02
F(neut) err	7.09E-04	3.72E-04	3.96E-03	3.92E-04	3.40E-04
F(neut) err %	0.6%	0.3%	3.3%	0.4%	0.4%
Vac Rack used	bottom arm, w/bulb	bottom arm, w/bulb	bottom arm, w/bulb	bottom arm, w/bulb	bottom arm, w/bulb
Vac Rack calib	10/6/2004	10/6/2004	10/6/2004	10/6/2004	10/6/2004
z	Varies	Varies	Varies	Varies	Varies
falloff	1.3	1.3	1.27	1.05	1.09
# of half-lives	0.38	0.35	0.35	0.08	0.13
Plot quality					
Comments					

k = 3.15E-12
std dev = 1.78307E-12
std dev (%) = 56.6%
Count = 5

alpha = 1.34E-23 **Source =** CRC 2000 Elect
dipole = 0.66 ± 0.05 **Source =** CRC 2000 Elect

k(ADO) = 1.11E-09 **Eff(ADO) =** 0.3%

k(SC) = 1.17E-09 **Eff(SC) =** 0.3%

Kinetic Plots for the Reaction of the Bis-trimethylsilylmethyloxonium Ion and Triethylamine

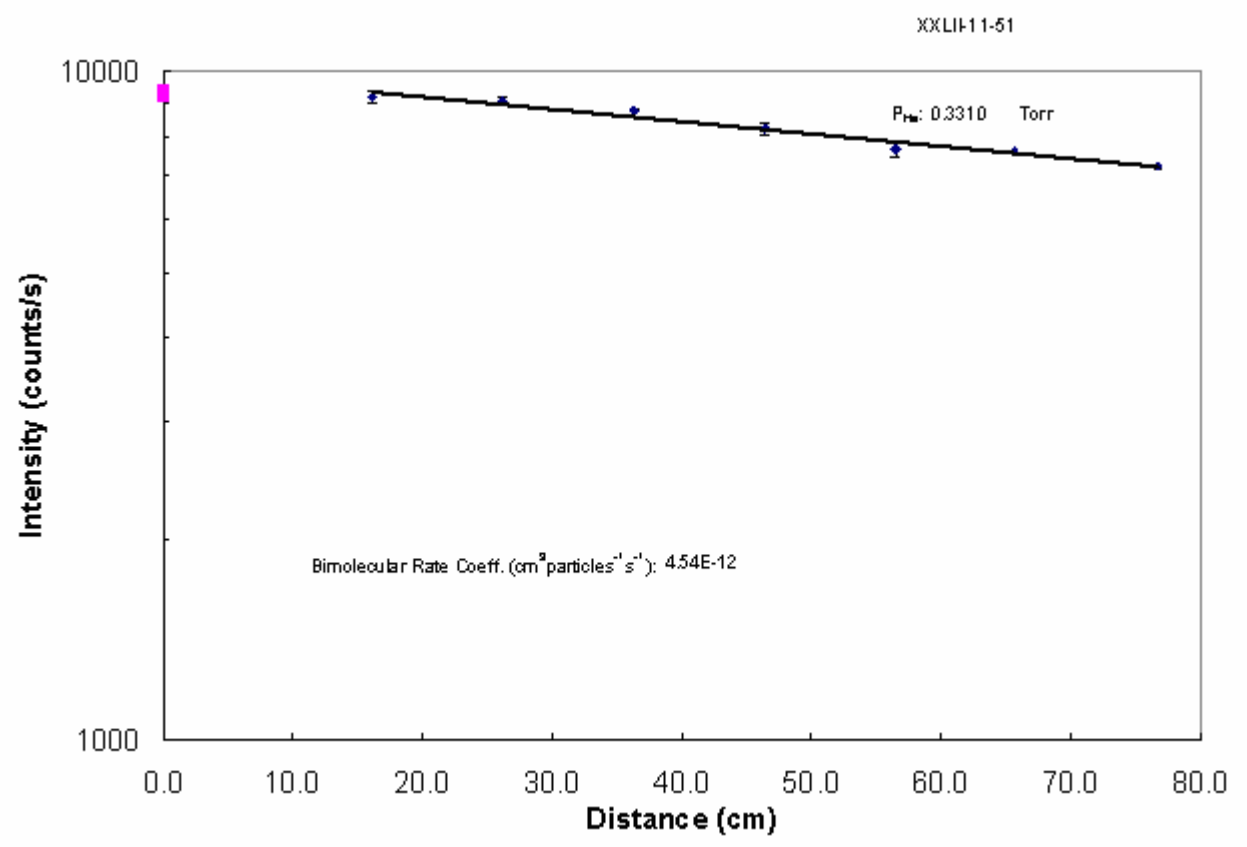

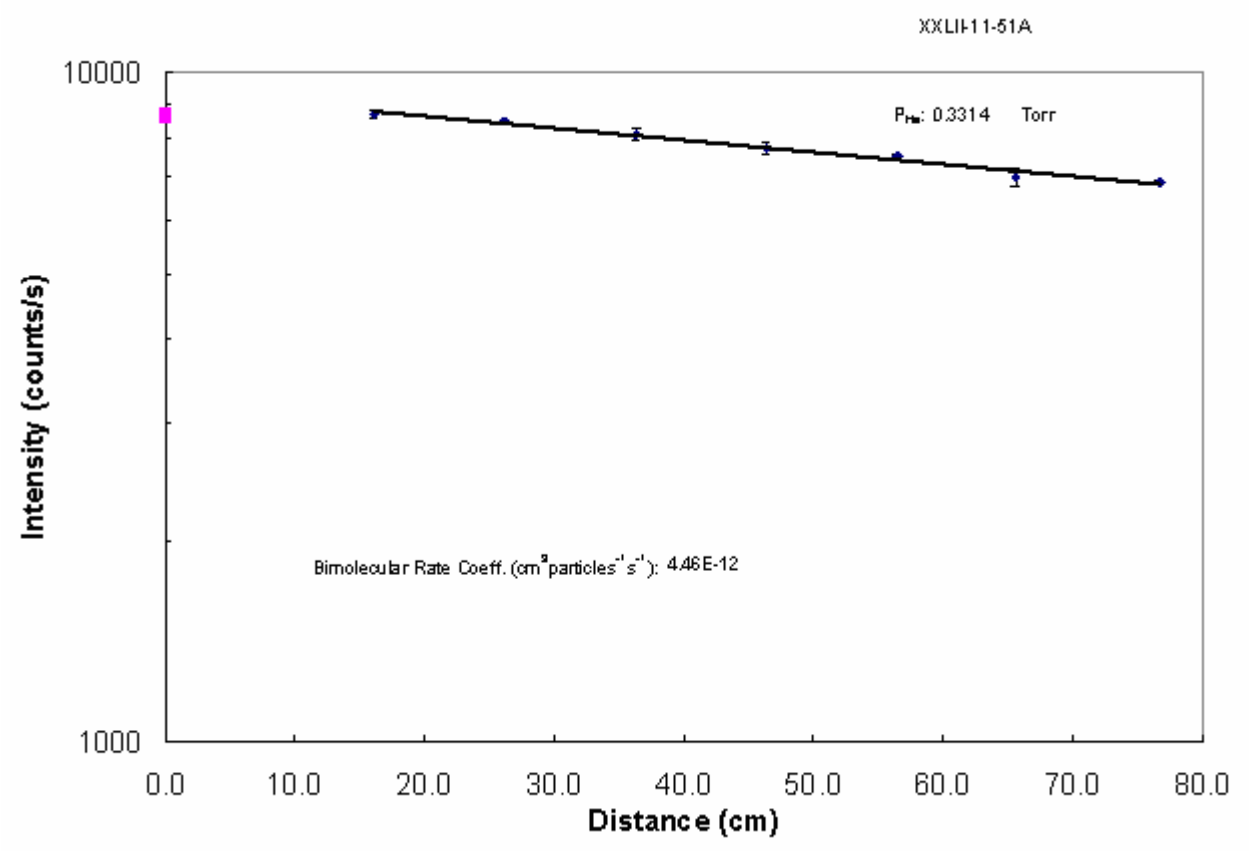
XXLII-11-51A
10000
1000
P_{He}: 0.3314 Torr
Bimolecular Rate Coeff. ($cm^3 particles^{-1} s^{-1}$): 4.46E-12
Intensity (counts/s)
0.0
10.0
20.0
30.0
40.0
50.0
60.0
70.0
80.0
Distance (cm)

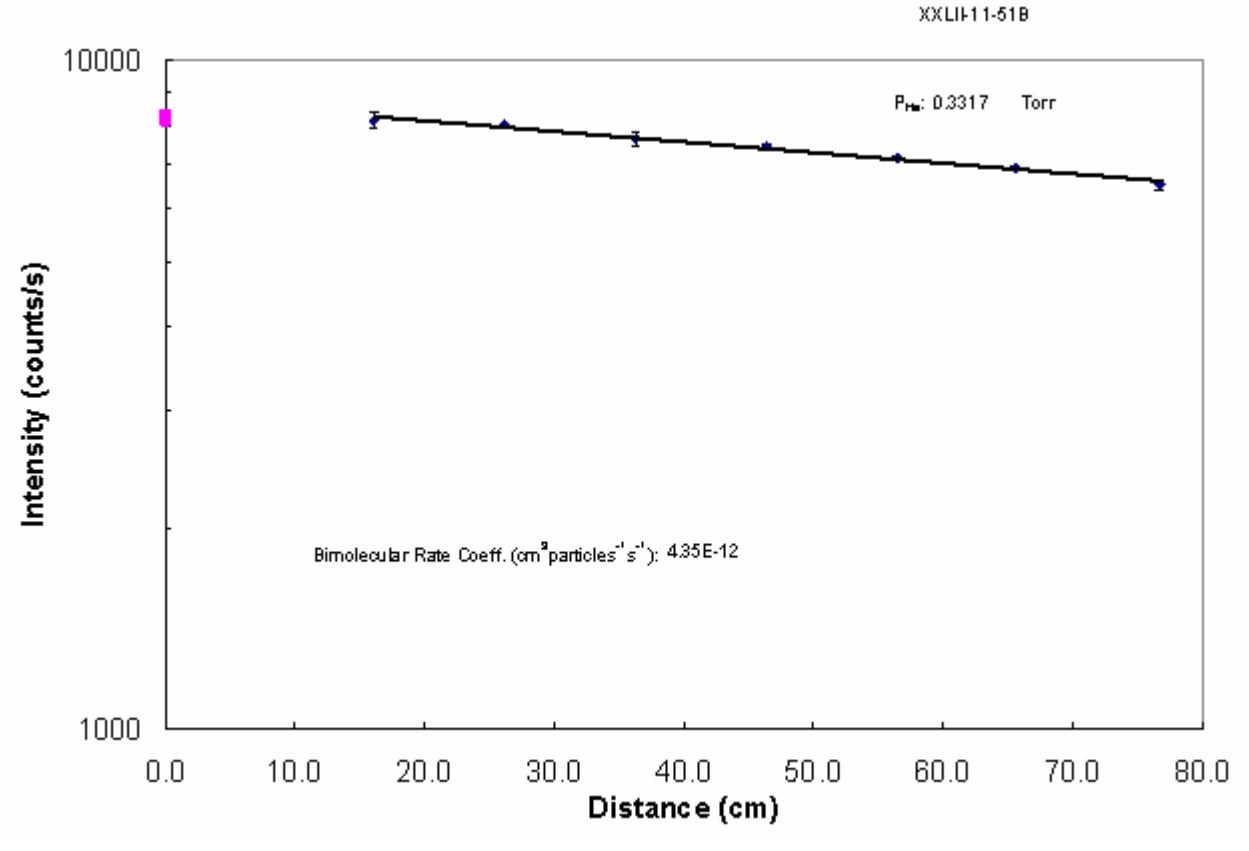
XXLII-11-51B
10000
1000
P_{He}: 0.3317 Torr
Bimolecular Rate Coeff. ($cm^3 particles^{-1} s^{-1}$): 4.35E-12
Intensity (counts/s)
0.0
10.0
20.0
30.0
40.0
50.0
60.0
70.0
80.0
Distance (cm)

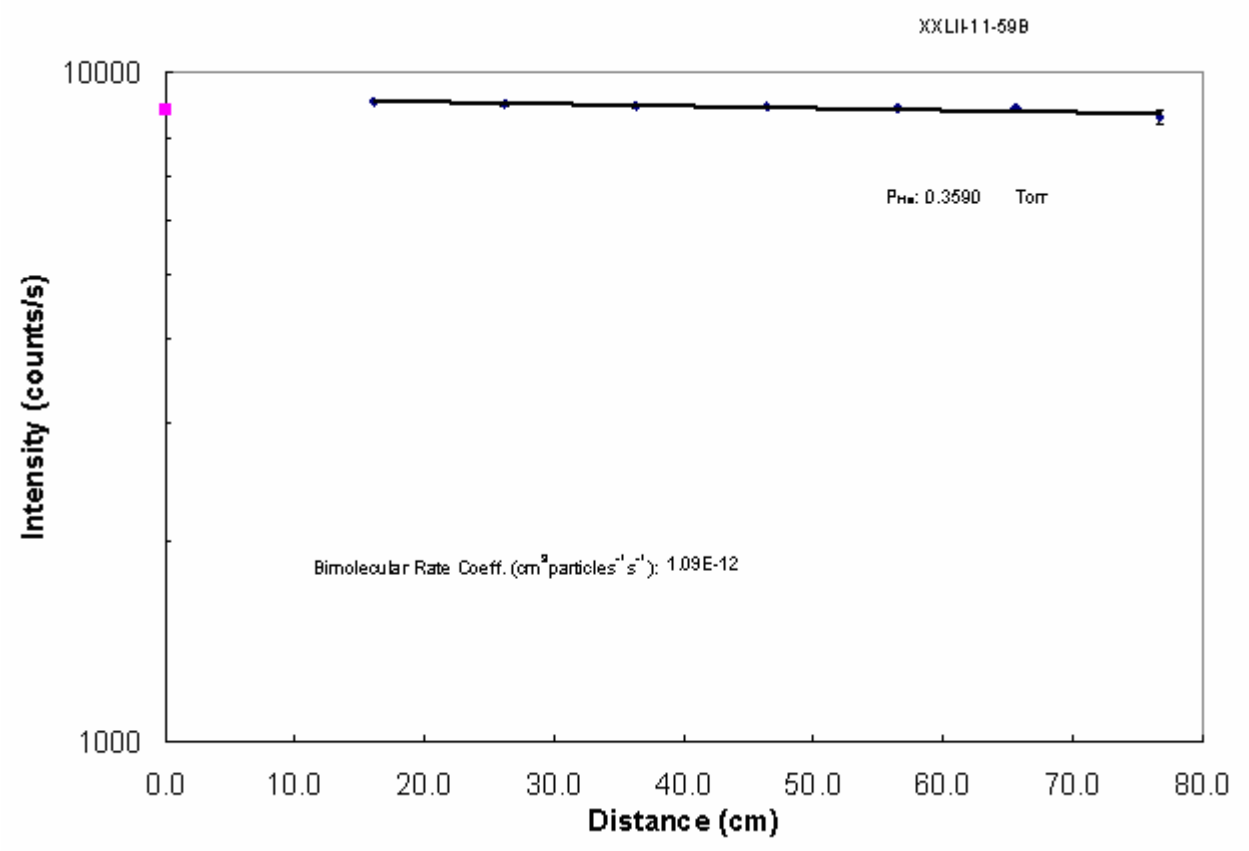
XXLII-11-59B
10000
1000
Intensity (counts/s)
P_{He}: 0.3590 Torr
Bimolecular Rate Coeff. ($cm^3 particles^{-1} s^{-1}$): 1.09E-12
0.0
10.0
20.0
30.0
40.0
50.0
60.0
70.0
80.0
Distance (cm)

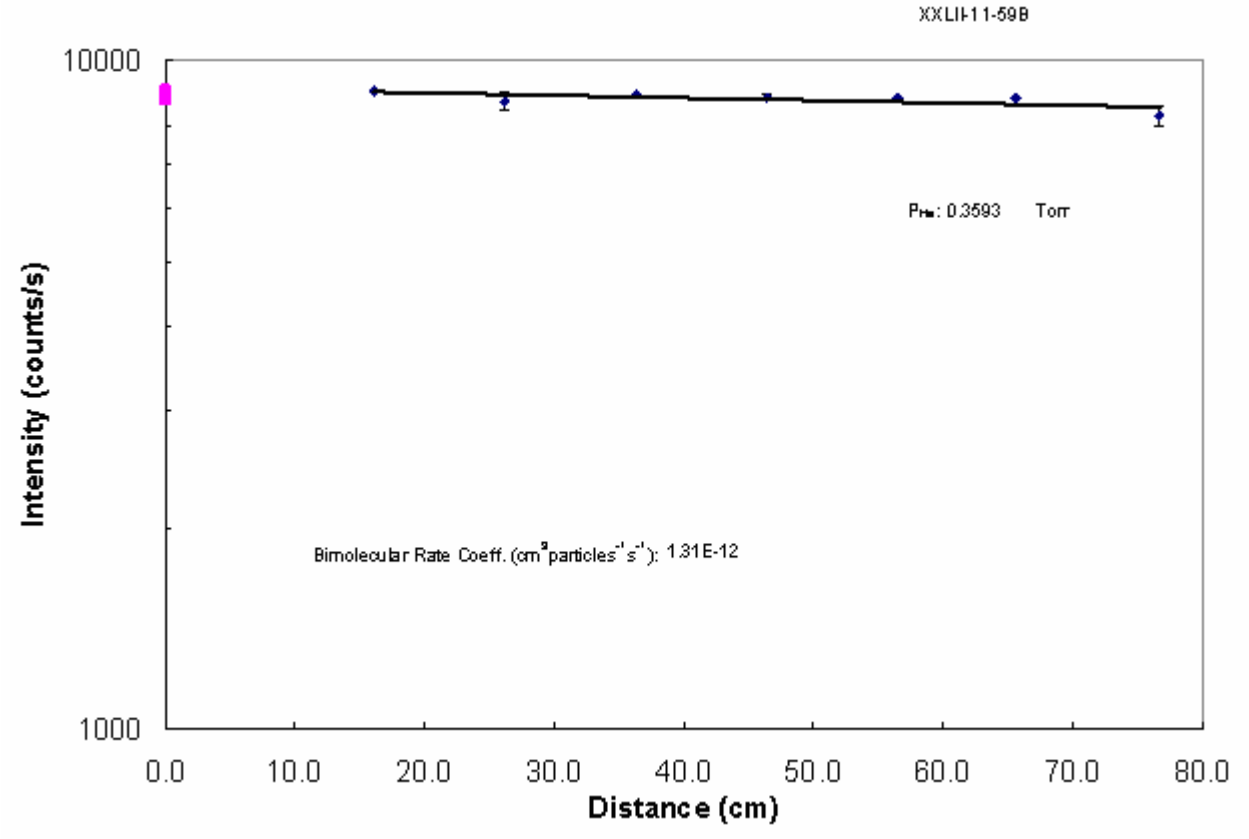
XXLII-11-59B
10000
1000
Intensity (counts/s)
P_{He}: 0.3593 Torr
Bimolecular Rate Coeff. ($cm^3 particles^{-1} s^{-1}$): 1.31E-12
0.0
10.0
20.0
30.0
40.0
50.0
60.0
70.0
80.0
Distance (cm)

STRUCTURES OF TRANSITION STATES AND COMPLEXES FOR THE REACTION OF $O^{\cdot-}$ WITH METHANOL

$CH3OO^-$

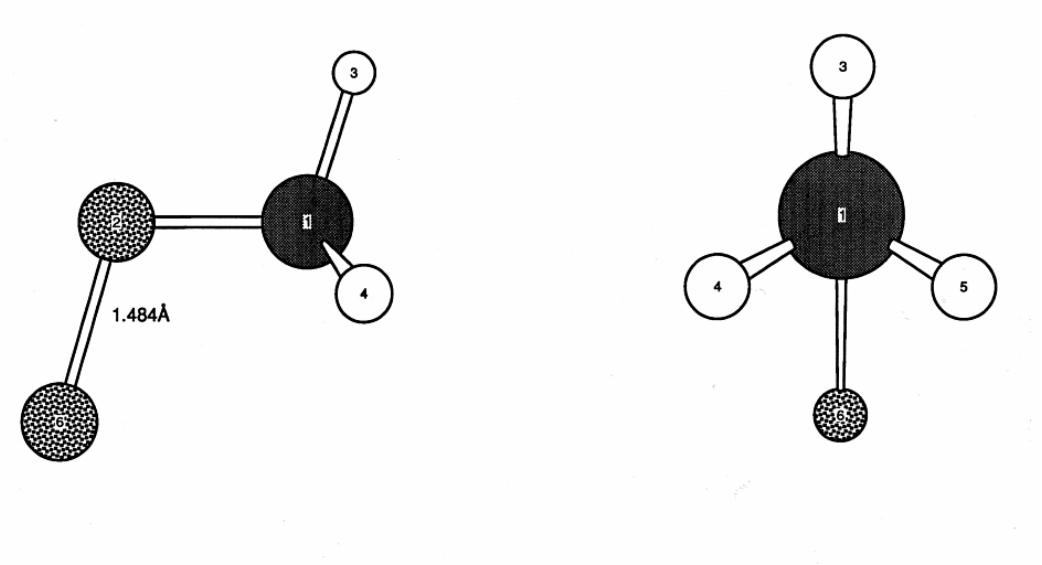

Complex 7

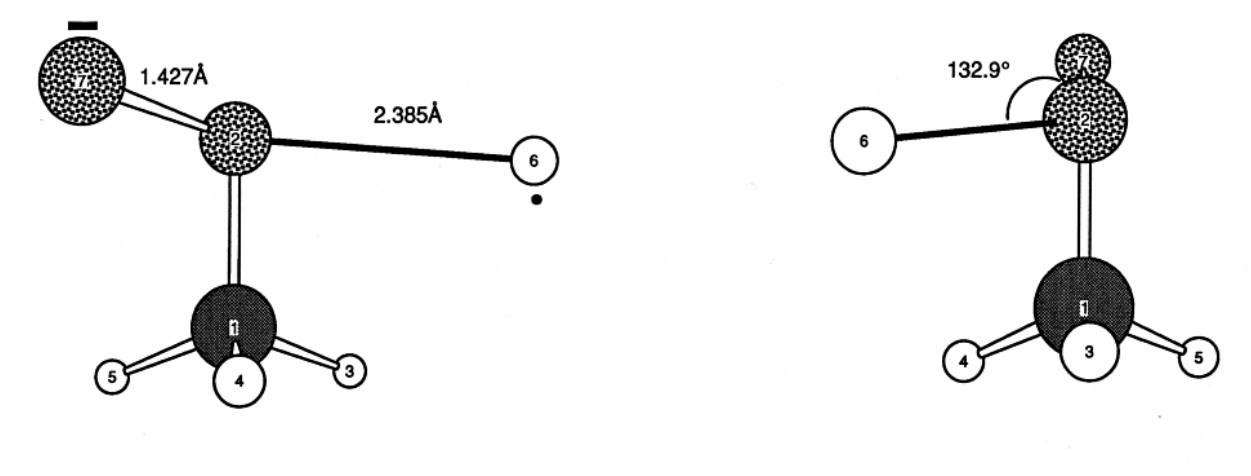

Total atomic charges:		Total atomic spin densities:	
	1		1
1 C	-.638295	1 C	.074927
2 O	-.004837	2 O	.062803
3 H	.158607	3 H	-.002940
4 H	.165141	4 H	.006450
5 H	.137519	5 H	-.007035
6 H	-.180091	6 H	.668695
7 O	-.638045	7 O	.197098

CH_3

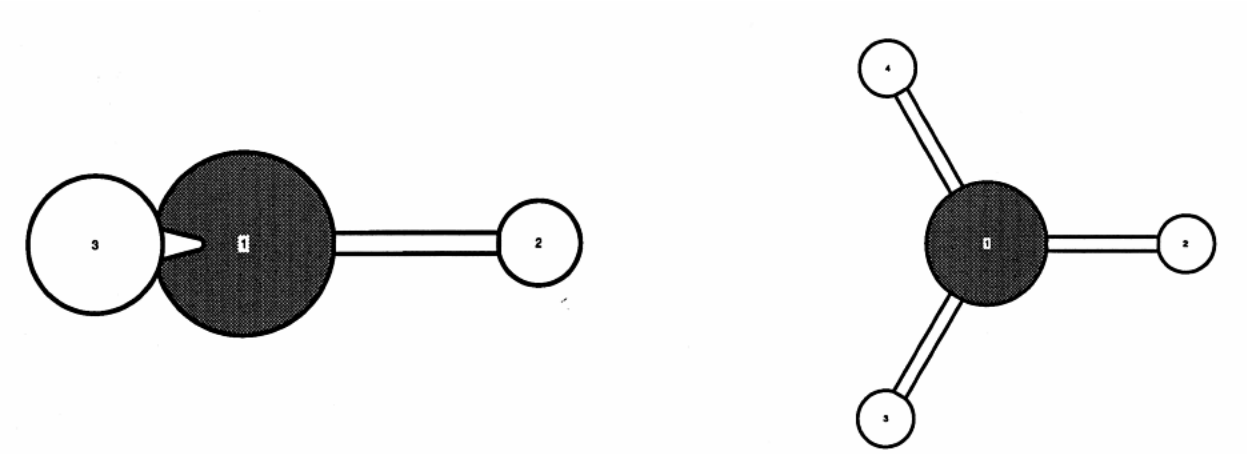

HOO^-

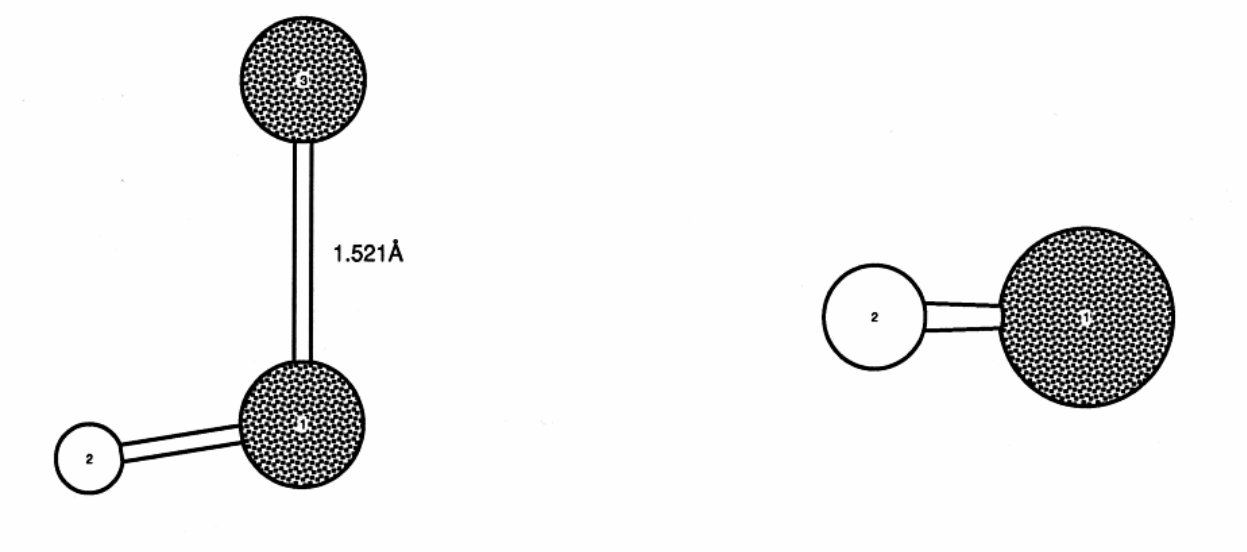

Complex 8

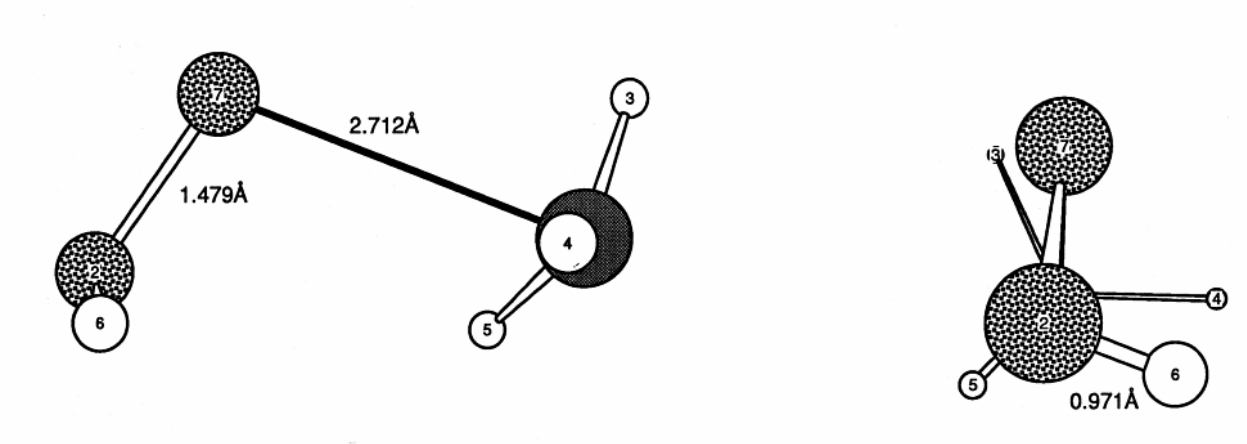

Total atomic charges:

		1
1	C	-.810661
2	O	-.567104
3	H	.160132
4	H	.158233
5	H	.210137
6	H	.413164
7	O	-.563901

Sum of Mulliken charges= -1.00000

Total atomic spin densities:

		1
1	C	.878608
2	O	.030016
3	H	-.029924
4	H	-.030157
5	H	-.026984
6	H	-.000343
7	O	.178784

Sum of Mulliken spin densities= 1.00000

CH_3O^- and HO

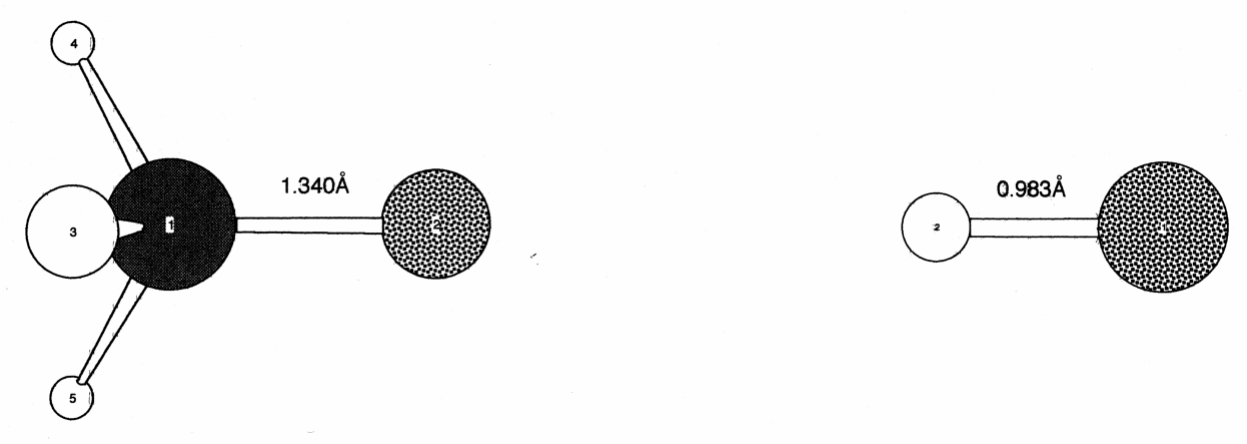

Total atomic charges:

		1
1	C	-.323809
2	O	-.825870
3	H	.049896
4	H	.049892
5	H	.049891

Total atomic spin densities:

		1
1	O	1.031889
2	H	-.031889

CH_3OH

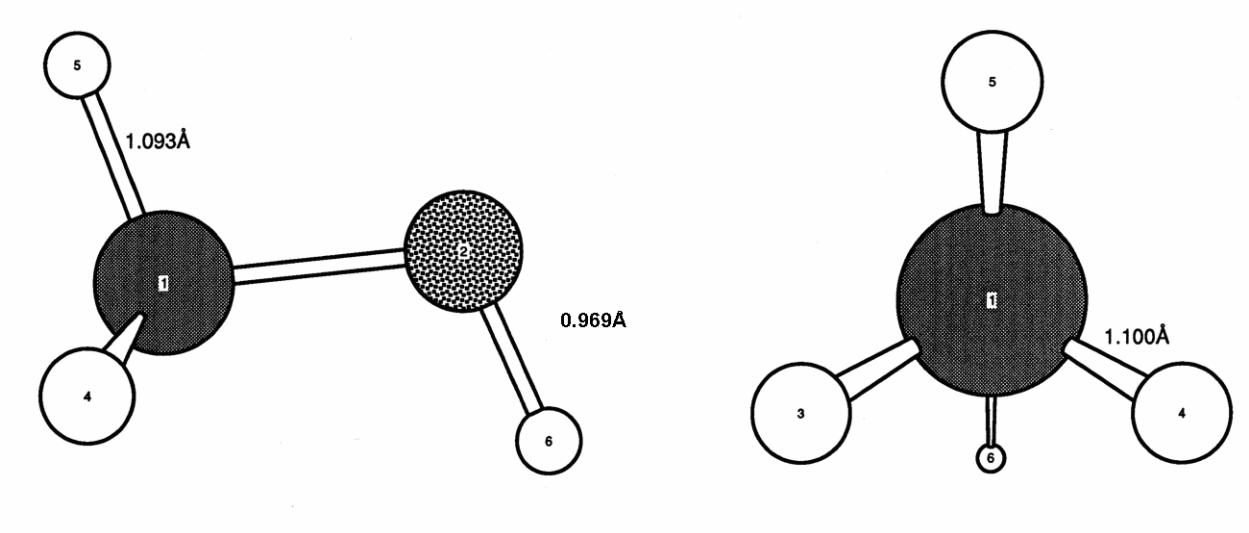

ts23

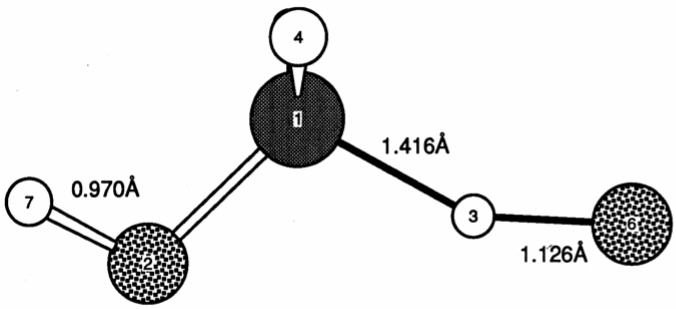

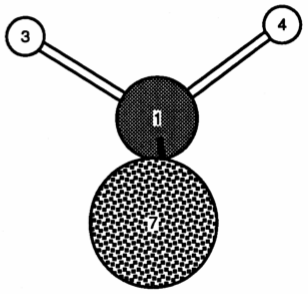

Total atomic charges:

		1
1	C	-.487079
2	O	-.650337
3	H	.401210
4	H	.137147
5	H	.132109
6	O	-.946877
7	H	.413828

Sum of Mulliken charges= -1.00000

Total atomic spin densities:

		1
1	C	.469815
2	O	-.014628
3	H	-.072951
4	H	-.017648
5	H	-.012009
6	O	.627779
7	H	.019643

Sum of Mulliken spin densities= 1.00000

Complex 2

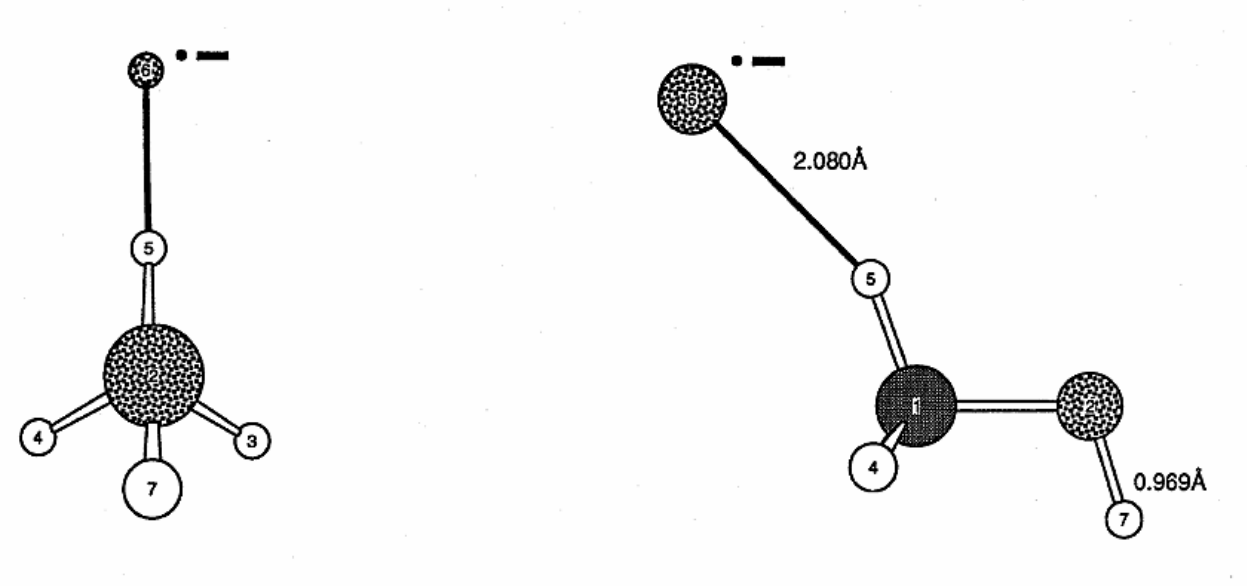

Total atomic charges:	
	1
1 C	-.454553
2 O	-.660573
3 H	.135813
4 H	.135813
5 H	.336575
6 O	-.907596
7 H	.414521

Total atomic spin densities:	
	1
1 C	-.010651
2 O	.002536
3 H	.000316
4 H	.000316
5 H	-.005734
6 O	1.013724
7 H	-.000506

CH_4

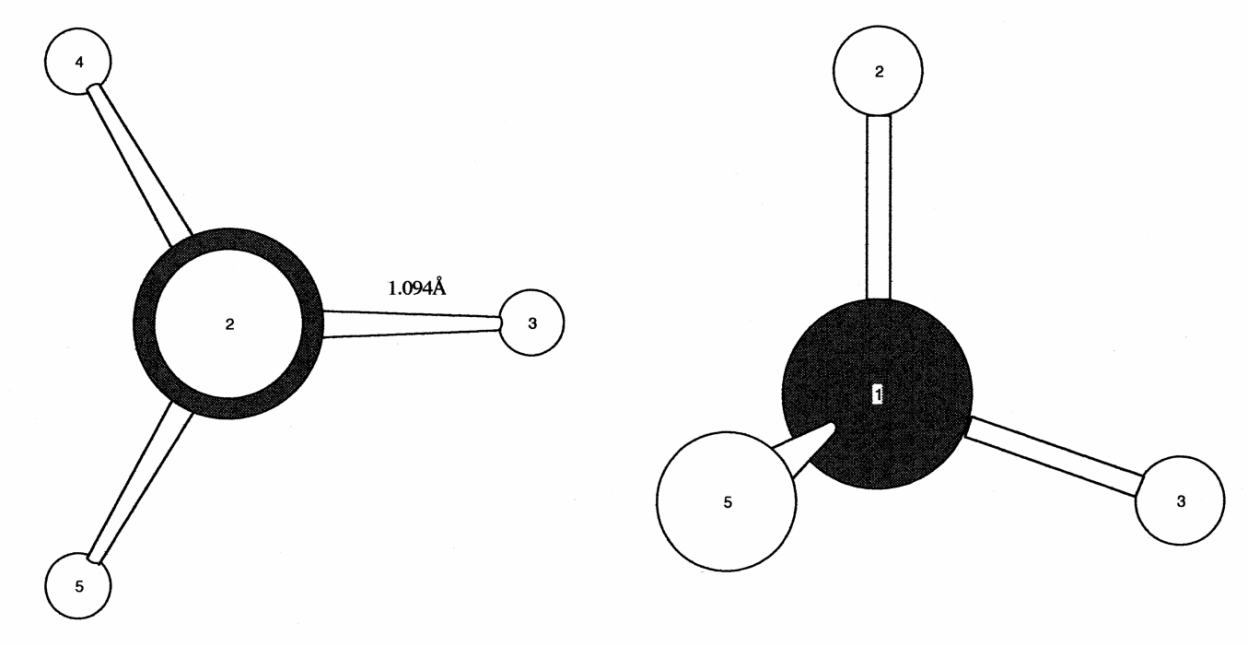

Total atomic charges:

		1
1	C	-.797955
2	H	.199501
3	H	.199485
4	H	.199485
5	H	.199485

O_2^-

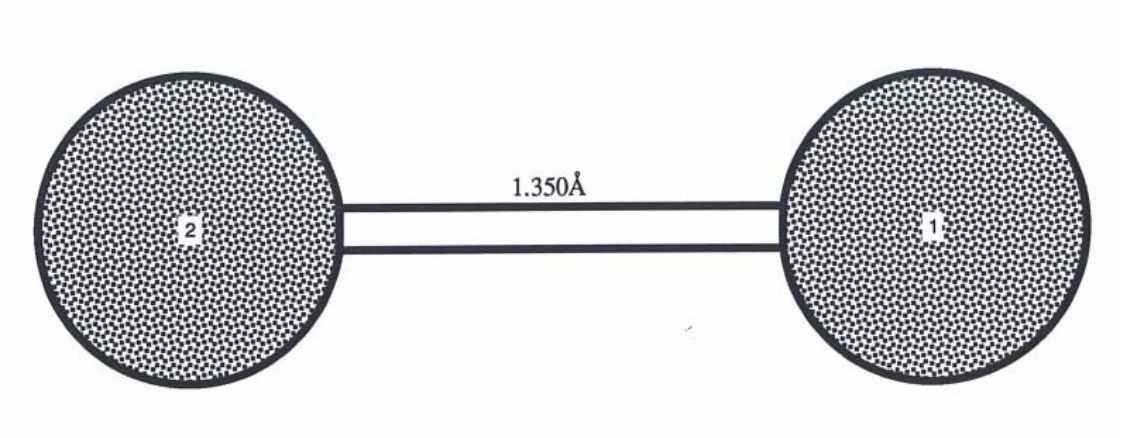

Total atomic charges:

		1
1	O	-.500000
2	O	-.500000

Sum of Mulliken charges= -1.00000

Total atomic spin densities:

		1
1	O	.500000
2	O	.500000

Sum of Mulliken spin densities= 1.00000

ts 59

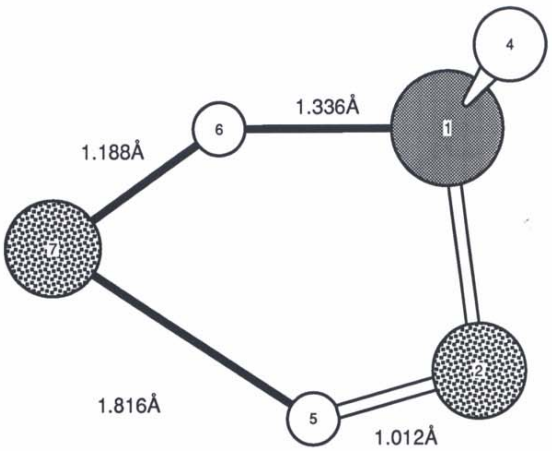

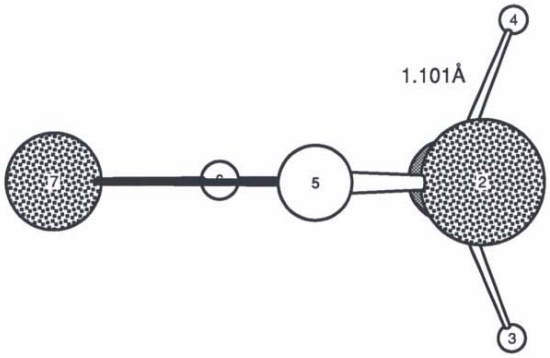

Total atomic charges:

		1
1	C	-.432664
2	O	-.646910
3	H	.331341
4	H	.125996
5	H	.126004
6	O	-.982966
7	H	.479199

Sum of Mulliken charges= -1.00000

Total atomic spin densities:

		1
1	C	.543640
2	O	.001956
3	H	-.099386
4	H	-.013578
5	H	-.013582
6	O	.578894
7	H	.002055

Sum of Mulliken spin densities= 1.00000

Complex 3

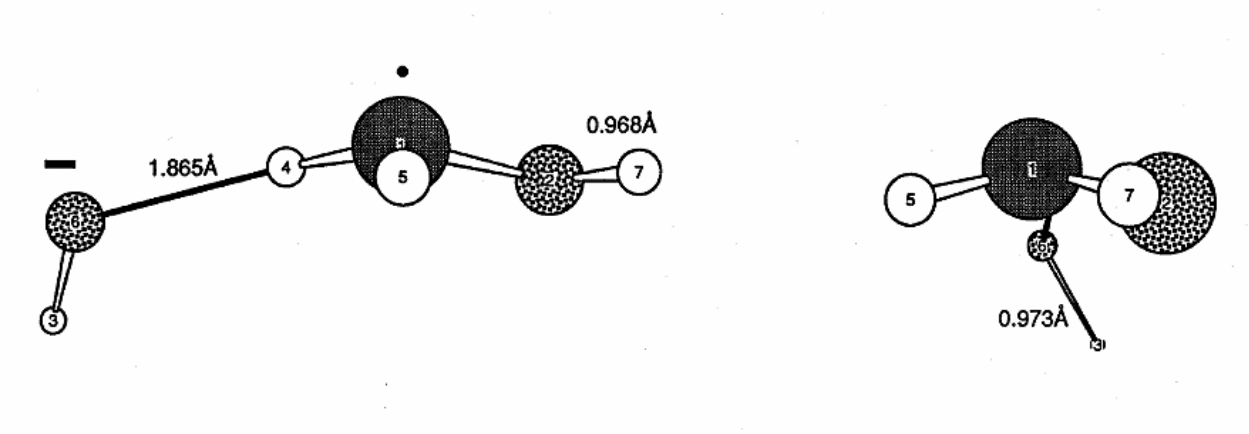

Total atomic charges:		Total atomic spin densities:	
	1		1
1 C	-.413109	1 C	.979307
2 O	-.574268	2 O	.068956
3 H	.352653	3 H	-.001238
4 H	.377118	4 H	-.035755
5 H	.103984	5 H	-.033472
6 O	-1.266626	6 O	.027502
7 H	.420247	7 H	-.005300

Complex 10

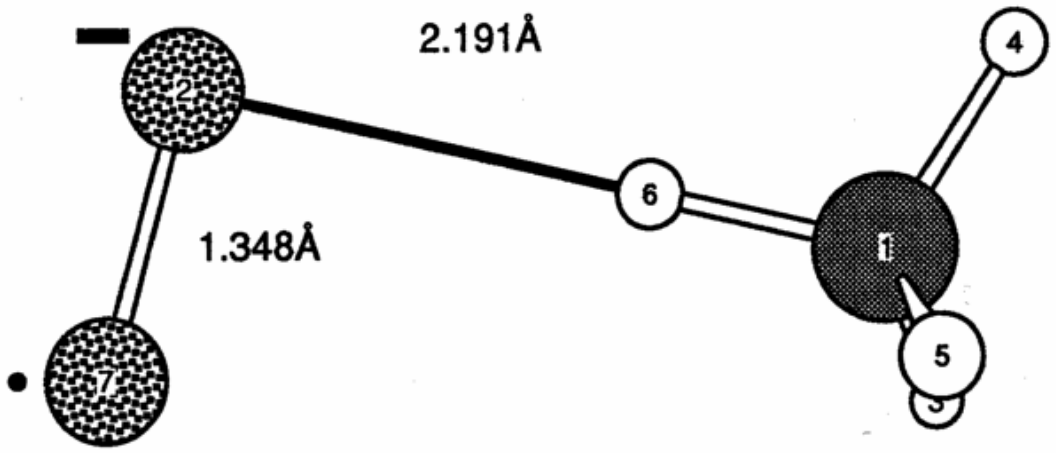

Total atomic charges:

		1
1	C	-.882954
2	O	-.461685
3	H	.160109
4	H	.152182
5	H	.156302
6	H	.341766
7	O	-.465721

Sum of Mulliken charges= -1.00000

Total atomic spin densities:

		1
1	C	-.012992
2	O	.503243
3	H	-.000237
4	H	.001257
5	H	-.000105
6	H	-.002852
7	O	.511686

Sum of Mulliken spin densities= 1.00000

Complex 1

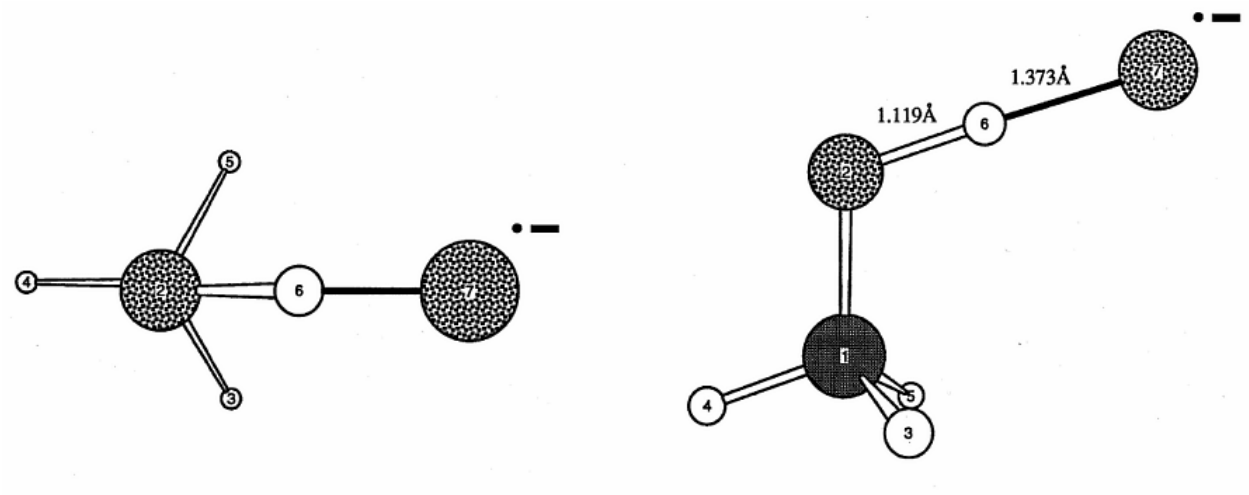

Total atomic charges:		Total atomic spin densities:	
	1		1
1 C	-.359266	1 C	-.006196
2 O	-.740981	2 O	.010078
3 H	.127789	3 H	.000803
4 H	.115168	4 H	-.000267
5 H	.127783	5 H	.000804
6 H	.527806	6 H	-.018481
7 O	-.798299	7 O	1.013258

Complex 4

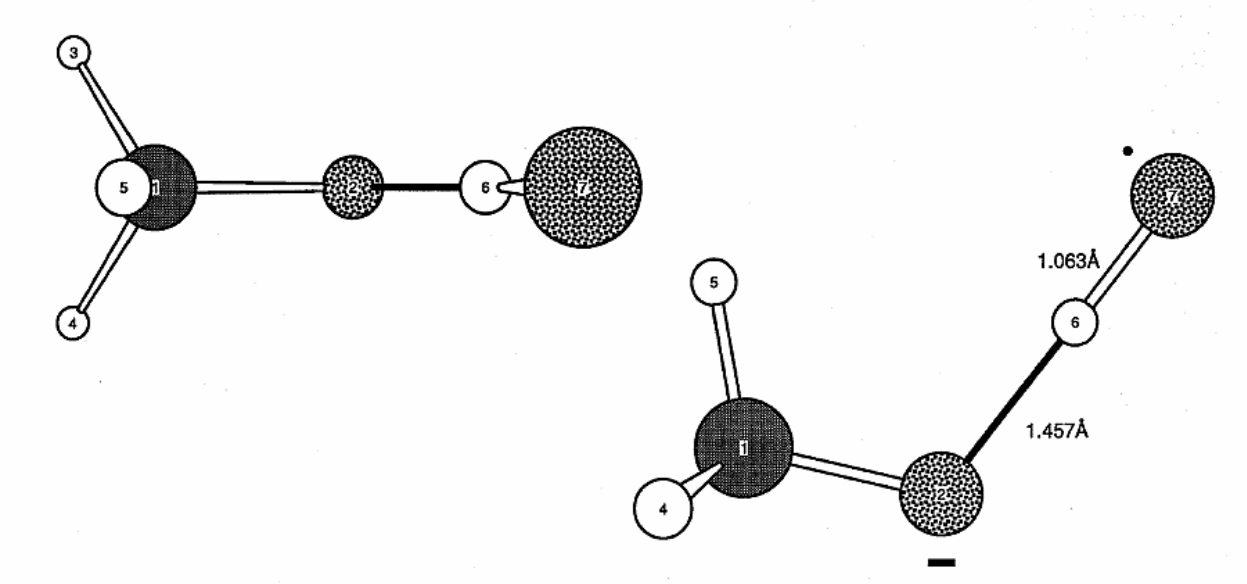

Total atomic charges:	
	1
1 C	-.334673
2 O	-.790798
3 H	.093132
4 H	.093132
5 H	.113772
6 H	.568561
7 O	-.743125

Total atomic spin densities:	
	1
1 C	-.004622
2 O	.080258
3 H	.005659
4 H	.005659
5 H	-.000787
6 H	-.020430
7 O	.934263

CH_2O

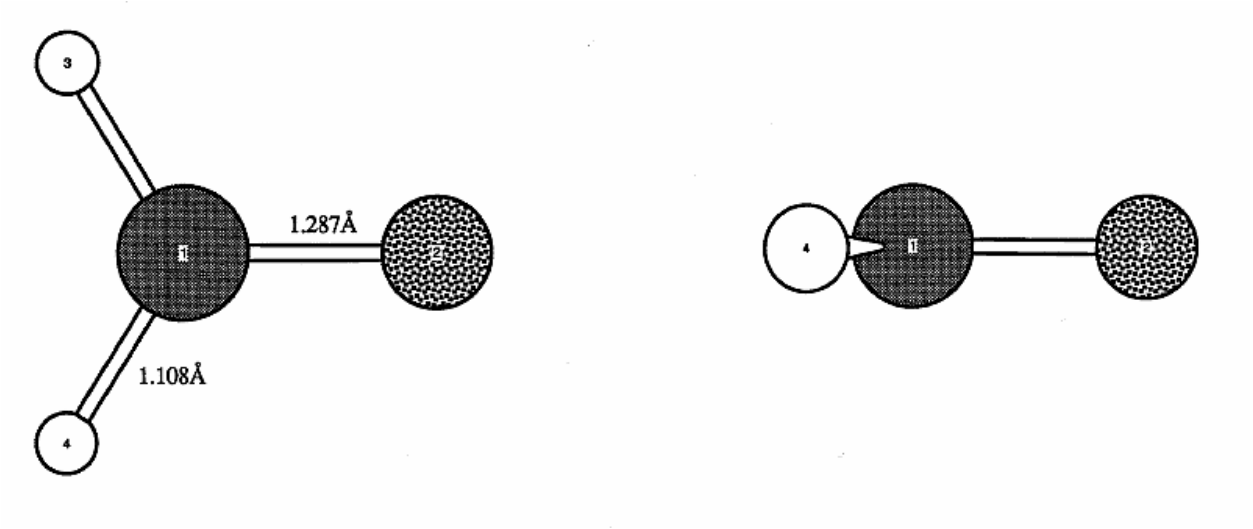

Total atomic charges:	
	1
1 C	-.639149
2 O	-.525390
3 H	.082269
4 H	.082269

Total atomic spin densities:	
	1
1 C	.855336
2 O	.207345
3 H	-.031341
4 H	-.031341

H_2O

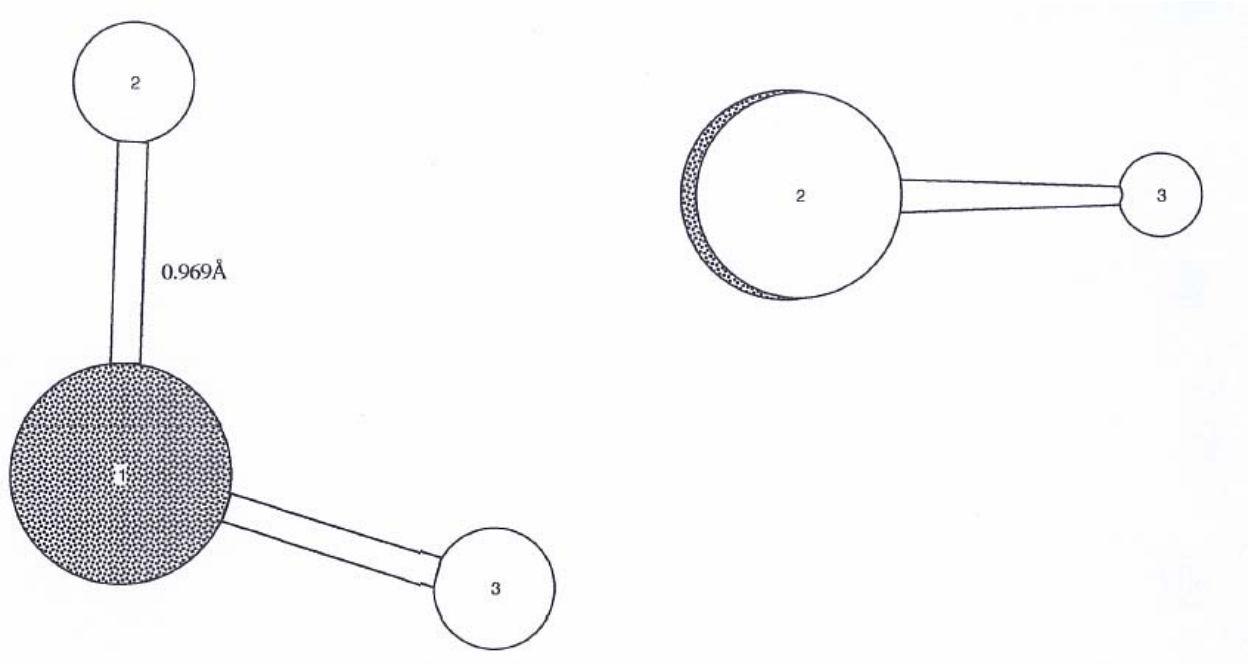

Total atomic charges:

		1
1	O	-.943759
2	H	.471879
3	H	.471879

Sum of Mulliken charges= .00000

Complex 9

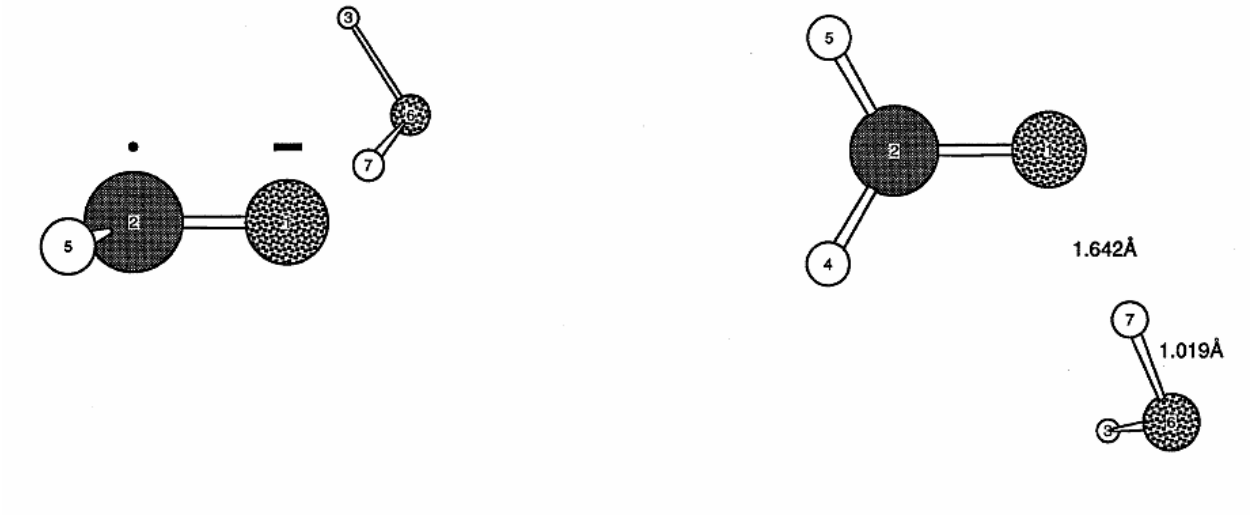

Total atomic charges:			Total atomic spin densities:		
		1			1
1	O	-0.599827	1	O	0.214304
2	C	-0.520464	2	C	0.846307
3	H	0.427643	3	H	0.001383
4	H	0.093697	4	H	-0.027671
5	H	0.089457	5	H	-0.029053
6	O	-1.067131	6	O	-0.002120
7	H	0.576626	7	H	-0.003150

BIBLIOGRAPHY

(1) Hogness, T. R.; Lunn, E. G. *Physical Review* **1925**, *26*, 44.

(2) Lias, S. G.; Ausloos, P. *Ion-Molecule Reactions, Their Role in Radiation Chemistry*; American Chemical Society: Washington, D.C., 1975.

(3) Norton, R. B.; Ferguson, E. E.; Fehsenfeld, F. C.; Schmeltekopf, A. L. *Planetary Space Sci.* **1966**, *14*, 969-978.

(4) Ferguson, E. E.; Fehsenfeld, F. C.; Schmeltekopf, A. L. *Advan. At. Mol. Phys.* **1969**, *5*, 1-56.

(5) Ferguson, E. E.; Fehsenfeld, F. C.; Albritton, D. L. In *Gas Phase Ion Chemistry*; Bowers, M. T., Ed.; Academic Press: New York, 1979; Vol. 1, pp 45-82.

(6) Depuy, C. H.; Grabowski, J. J.; Bierbaum , V. M. *Science* **1982**, *218*, 955-960.

(7) Mackay, G. I.; Bohme, D. K. *Journal of the American Chemical Society* **1978**, *100*, 327-329.

(8) Frisch, M. J.; Trucks, G. W.; Schlegel, H. B.; Scuseria, G. E.; Robb, M. A.; Cheeseman, J. R.; Montgomery, J. A. J.; Vreven, T.; Kudin, K. N.; Burant, J. C.; Millam, J. M.; Iyengar, S. S.; Tomasi, J.; Barone, V.; Mennucci, B.; Cossi, M.; Scalmani, G.; Rega, N.; Petersson, G. A.; Nakatsuji, H.; Hada, M.; Ehara, M.; Toyota, K.; Fukuda, R.; Hasegawa, J.; Ishida, M.; Nakajima, T.; Honda, Y.; Kitao, O.; Nakai, H.; Klene, M.; Li, X.; Knox, J. E.; Hratchian, H. P.; Cross, J. B.; Adamo, C.; Jaramillo, J.; Gomperts, R.; Stratmann, R. E.; Yazyev, O.; Austin, A. J.; Cammi, R.; Pomelli, C.; Ochterski, J. W.; Ayala, P. Y.; Morokuma, K.; Voth, G. A.; Salvador, P.; Dannenberg, J. J.; Zakrzewski, V. G.; Daniels, A. D.; Farkas, O.; Rabuck, A. D.; Raghavachari, K.; Ortiz, J. V.; 6.0 ed.; Gaussian Inc: Pittsburgh, 2003.

(9) Fujitsu; 6.1 ed.; Oxford Molecular Ltd., 2000-2004.

(10) Alcami, M.; Mo, O.; Yanez, M. *Mass Spectrometry Reviews* **2001**, *20*, 195-245.

(11) Alcami, M.; Mo, O.; Yanez, M. *Mass Spectrometry Review* **2001**, *20*, 195-245.

(12) Srikanth, R.; Reddy, P. N.; Bhanuprakash, K.; Srinivas, R.; Chen, X.; Turecek, F. *American Society for Mass Spectrometry* **2005**, *16*, 1353-1366.

(13) Zhao, J.; Zhang, R. *Atmospheric Environment* **2004**, *38*, 2177-2185.

(14) Fleming, I. *Chem. Soc. Rev.* **1981**, *10*, 83-111.

(15) Hwu, J. R.; Wetzel, J. M. *Journal of Organic Chemistry* **1985**, *50*, 3946-3948.

(16) Olah, G. A.; Li, X.; Wang, Q.; Rasul, G.; Prakash, G. K. S. *Journal of the American Chemical Society* **1995**, *117*, 8962-8966.

(17) Melley, S. J.; Grabowski, J. J. *International Journal of Mass Spectrometry and Ion Process* **1987**, *81*, 147-164.

(18) Chen, Q.-F.; Stone, J. A. *Int. J. Mass Spectrom. Ion Proc.* **1997**, *165/166*, 195-207.

(19) Squires, R. R.; Wang, D.; Farcasiu, D. *International Journal of Mass Spectrometry and Ion Process* **1991**, *107*, R7-R10.

(20) Lidstrom, P. J.; Mallard, W. G., Eds. *NIST Chemistry WebBook, NIST Standard Reference Database Number 69*; March 2003 ed.; National Institute of Standards and Technology: Gaithersburg MD, 20899, 2003.

(21) Fehsenfeld, F. C.; Schmeltekopf, A. L.; Schiff, H. I.; Ferguson, E. E. *Planet. Space Sci.* **1966**, *15*, 373-379.

(22) Lee, J.; Grabowski, J. J. *Chemical Reviews* **1992**, *92*, 1611-1647.

(23) Ramos, L. E.; Cardoso, A. M.; Ferrer-Correia, A. J. *Advances in Mass Spectrometry* **2001**, *15*, 731-732.

(24) Lin, M.; Grabowski, J. J. *International Journal of Mass Spectrometry* **2004**, *237*, 149-165.

(25) Melly, S. J.; Grabowski, J. J. *Int. J. Mass Spectrom. Ion Proc.* **1987**, *81*, 147-164.

(26) Clifford, E. P.; Wenthold, P. G.; Lineberger, W. C.; Ellison, G. B.; Wang, C. X.; Grabowski, J. J.; Vila, F.; Jordan, K. D. *Perkin Transactions 2* **1998**, 1015-1022.

(27) Futrell, J. H.; Tiernan, T. O. In *Ion Molecule Reactions*; Franklin, J. L., Ed.; Plenum Press: New York, 1972; Vol. 2, p 485.

(28) Jager, K.; Simic, M.; Henglein, A. *Zeitschrift fuer Naturforschung, Teil A: Astrophysik, Physik, und Physikalische* **1967**, *22*, 961-965.

(29) Houriet, R.; Stahl, D.; Winkler, F. J. *Environmental Health Perspectives* **1980**, *36*, 63-68.

(30) Boand, G.; Houriet, R.; Gaumann, T. In *Advances in Mass Spectrometry*; Quayle, A., Ed.; Heyden and Son LTD: Lausanne, Switzerland, 1980; Vol. 8a, pp 238-245.

(31) Frisch, M. J.; Trucks, G. W.; Schlegel, H. B.; Gill, P. M. W.; Johnson, B. G.; Robb, M. A.; Chesseman, J. R.; Keith, T.; Petersson, G. A.; Montgomery, J. A.; Raghavachari, K.; Al-Laham, M. A.; Zakrzewski, V. G.; Ortiz, J.; Gaussian, Inc: Pittsburgh, 1994.

(32) Hohenberg, P.; Kohn, W. *Phys. Rev.* **1964**, *B*, 864.

(33) Kohn, W.; Sham, L. J. *Phys. Rev.* **1965**, *A*, 1133.

(34) Becke, A. D. *J. Chem. Phys.* **1993**, 5648.

(35) Lee, C.; Yang, W.; Parr, R. G. *Phys. Rev.* **1988**, *B*, 785.

(36) Ishida, K.; Morokuma, K.; Kormornicki, A. *J. Chem. Phys.* **1977**, 2153.

(37) Gonzalez, C.; Schlegel, H. B. *J. Chem. Phys.* **1989**, 2154.

(38) Gonzalez, C.; Schlegel, H. B. *J. Chem. Phys.* **1990**, 5523.